RATE ADAPTIVE OFDMA COMMUNICATION SYSTEMS

By

Mai Mahmoud Mohammed Mahmoud Abdelhakim

National Center for Radiation Research & Technology (NCRRT)

Atomic Energy Authority

A Thesis Submitted to the

Faculty of Engineering at Cairo University

in Partial Fulfillment of the

Requirement for the Degree of

MASTER OF SCIENCE

in

ELECTRONICS AND COMMUNICATIONS ENGINEERING

FACULTY OF ENGINEERING, CAIRO UNIVERSITY

GIZA, EGYPT

April 2009

RATE ADAPTIVE OFDMA COMMUNICATION SYSTEMS

By

Mai Mahmoud Mohammed Mahmoud Abdelhakim

A Thesis Submitted to the
Faculty of Engineering at Cairo University
in Partial Fulfillment of the
Requirement for the Degree of
MASTER OF SCIENCE
in
ELECTRONICS AND COMMUNICATIONS ENGINEERING

Under the Supervision of

Ahmed Shalash
Associate professor, Electronics and Communications Department,
Faculty of engineering, Cairo University

Ayman Elezabi
Assistant professor, Electronics Engineering Department,
American University in Cairo

FACULTY OF ENGINEERING, CAIRO UNIVERSITY
GIZA, EGYPT
April 2009

RATE ADAPTIVE OFDMA COMMUNICATION SYSTEMS

By

Mai Mahmoud Mohammed Mahmoud Abdelhakim

A Thesis Submitted to the
Faculty of Engineering at Cairo University
in Partial Fulfillment of the
Requirement for the Degree of
MASTER OF SCIENCE
in
ELECTRONICS AND COMMUNICATIONS ENGINEERING

Approved by the Examining Committee:

_____
Prof. Esssam Sourour, Member (Alexandria University)

_____
Associate Prof. Mohammed Nafie, Member (Cairo University)

_____
Associate Prof. Ahmed Shalash, Thesis Main Advisor (Cairo University)

FACULTY OF ENGINEERING, CAIRO UNIVERSITY
GIZA, EGYPT
April 2009

ACKNOWLEDGEMENT

I would like to thank my supervisors, Dr. Ahmed Shalash and Dr. Ayman Elezabi, for their help and guidance throughout this work. Working with them was such a rewarding experience for me.

I would like to show my sincere appreciation to Dr. Mohammed Nafie for his technical and scientific support that had helped me a lot in progressing this work. I appreciate the valuable advices and support of Dr. Mohammed Khairy. I am also grateful to Prof. Mahmoud Ashour for his understanding and concern.

I can never forget to thank my friends, Aya and Hoda, for their encouragement and help.

I want to express my profound gratitude to my parents for their continuous love and support. Finally, I would also like to thank my dear fiancé for his encouragement, care and moral support.

Table of Contents

List of Figures

List of Tables

List of Symbols

SNR_{eff}	:	Effective SNR.
SNR_i	:	SNR of the i^{th} carrier.
N_c	:	Number of subcarriers.
β	:	Adjustable parameter used in the EESM scheme.
N_{EP}	:	Number of information bits input to the CTC encoder
N	:	Turbo block size
Sc	:	Circulation state
$S0_{N-1}$	:	Final state
A, B	:	Systematic subblocks output of the CTC encoder.
$Y1, Y2, W1, W2$	:	Four parity subblocks output of the CTC encoder.
SI	:	Symbol mutual information.
C_d	:	Total number of information bit errors produced by the all incorrect paths of weight d that diverge from the correct path then remerge to it later.
X_d	:	Total number of incorrect paths of a distance d that diverge from the correct path then remerge to it later.
A_d	:	Number of error events of weight d that diverge from the correct path at each node and remerge at the correct path later. Shifted codwords are considered once in A_d
P_d	:	Probability of deciding an incorrect path which is the pairwise error probability.
d_{free}	:	Minimum distance of the code.
B_i	:	Total number of information bits in the codeword for the i^{th} channel realization.
L	:	Coded bits in the codeword.

W	:	Total number of transmitted symbols in a codeword.
Z_i	:	Number of information bits of the i^{th} tile knowing the MCS assigned to it.
α	:	Index to the MCS.
GP_α	:	Goodput when the MCS at index α is used.
PER_α	:	PER when the MCS at index α is used.
I_α	:	Number of information bits if the MCS at index α is used.
η	:	Simulated goodput.
η_{max}	:	Maximum simulated goodput.
C	:	Number of channel realizations.
TER_t	:	Estimated PER for tile *t.*
T	:	Number of tiles.
$PER_{est,i}$	:	Estimated PER for the i^{th} channel realization
GP_{est}	:	Estimated goodput.
x	:	Transmitted signal
u:	:	Zero mean complex Gaussian noise
σ^2	:	Noise variance
Es	:	Symbol energy.
y	:	Received signal
$M(y/x)$	:	Log likelihood function of y given x.
Pr(x)	:	Probability of x.
H	:	Frequency response of the fading channel.

List of Abbreviations

AMC	:	Adaptive modulation and coding
BER	:	Bit error rate
CSI	:	Channel state information
CTC	:	Convolutional Turbo code
EESM	:	Exponential effective SINR mapping
ESM	:	Effective SINR mapping.
IntP	:	Interleaved puncturing.
LQM	:	Link quality metric
MCS	:	Modulation ad coding scheme
MCWs	:	Multiple CodeWords
MIESM	:	Mutual information effective SINR mapping
OFDM	:	Orthogonal frequency division multiplexing
OFDMA	:	Orthogonal frequency division multiple access
PDI	:	Puncturing dependant interleaving.
PER	:	Packet error rate
PFA	:	Per-Frame Adaptation
R-MIESM	:	Recursive mutual information effective SINR mapping.
SCW	:	Single CodeWord
SNR	:	Signal to Noise Ratio

ABSTRACT

Due to the varying nature of the wireless channels, adapting the transmission parameters, such as code rate, modulation order and power, in response to the channel variations provides a significant improvement in the system performance. In the OFDM systems, Per-Frame adaptation (PFA) can be employed where the transmission variables are fixed over a given frame and may change from one frame to the other. Subband (tile) loading offers more degrees of adaptation such that each group of carriers (subband) uses the same transmission parameters and different subbands may use different parameters. Changing the code rate for each tile in the same frame, results in transmitting multiple codewords (MCWs) for a single frame.

In this thesis a scheme is proposed for adaptively changing the code rate of coded OFDMA systems via changing the puncturing rate within a single codeword (SCW). In the proposed structure, the data is encoded with the lowest available code rate then it is divided among the different tiles where it is punctured adaptively based on some measure of the channel quality for each tile. The proposed scheme is compared against using multiple codewords (MCWs) where the different code rates for the tiles are obtained using separate encoding processes.

For bit interleaved coded modulation architecture two novel interleaving methods are proposed, namely the puncturing dependant interleaver (PDI) and interleaved puncturing (IntP), which provide larger interleaving depth. In the PDI method the coded bits with the same rate over different tiles are grouped for interleaving. In IntP structure the interleaving is performed prior to puncturing.

The performance of the adaptive puncturing technique is investigated under constant bit rate constraint and variable bit rate. Two different adaptive modulation

and coding (AMC) selection methods are examined for variable bit rate adaptive system. The first is a recursive scheme that operates directly on the SNR whereas the second operates on the effective SNR value that is obtained using Mutual Information Effective SNR Mapping (MIESM). We also propose a novel rate selection scheme for the SCW termed as Recursive Mutual Information Effective SNR mapping (R-MIESM) scheme and compare it against the MIESM scheme using Turbo codes. The R-MIESM scheme provides further goodput performance gains over the MIESM scheme. In the simulations the SCW is compared against the PFA where we fix the modulation and coding scheme (MCS) over a given frame. The simulations show that the proposed adaptive puncturing method of SCW is superior to the PFA and MCWs structure using Turbo or Convolutional codes.

CHAPTER 1
INTRODUCTION

Wireless standards aim at improving the spectral efficiency while maintaining their quality of service (QoS) requirements. One of the obstacles to wireless communications is the operation in a fading environment. Fading channels are time and frequency varying channels; they may vary during wireless transmission.

Due to the varying nature of the fading channels, it is inefficient to have fixed transmission parameters during wireless communication. If fixed transmission is employed, the operating parameters should be set according to the worst channel conditions. Thus, the radio will not benefit from the good environmental conditions when they occur. Allocation of resources is required to be adapted according to the channel variations in order to have efficient utilization of the available spectrum, consequently improving the overall system performance. Adaptation requires an intelligent radio that gets acquainted with the channel conditions and changes the transmission parameters accordingly. This requires channel estimation, channel prediction and feedback channel between the transmitter and the receiver.

The adaptive process operates according to a well defined loading scheme that acts upon the channel variations. Different adaptive loading schemes are present to direct the transmission variables (e.g. modulation order, code rate/scheme, transmission power etc.) towards maximizing the spectral efficiency of the system while preserving the QoS requirements defined for the application. The rate at which the transmission variables should change depends on how fast the channel varies.

Adaptation can be employed in single carrier and multi-carrier systems. For the single carrier systems the operating parameters are determined for each transmission. However, for multi-carrier systems the different subcarriers in the same OFDM frame may experience different channel depending on the channel frequency response. Adapting the OFDM system to the wireless environment could be applied on a per frame basis, per subcarrier basis, or on a per subband basis. A subband, which is also referred to as a resource block, is a group of subcarriers over several OFDM symbols. If those subcarriers are contiguous in both time and frequency, the resource block is called a physical resource block or "tile". Subband, resource block and a tile are used interchangeably in the thesis.

Adapting the OFDM system on a per frame basis, the transmission parameters are unchanged over the whole OFDM frame and may change from one frame to the other. A subcarrier by subcarrier loading improves the performance greatly at the expense of the increased system overhead needed to exchange the channel information at each subcarrier. Less efficient, though still powerful, loading is to have a subband adaptation. The overhead introduced by the subband adaptation is lower than the per-subcarrier loading since no precise information is needed for each subcarrier; instead a single metric indicating the channel quality for each subband is required. Subband adaptation is also referred to as zone loading in this thesis.

1.1. Scope of the work

In this thesis a novel structure for rate-adaptive coded OFDMA systems based on Subband adaptation is introduced. The proposed structure employs a Single CodeWord (SCW) over the OFDM frame, while providing different transmission rates over tiles via adaptive puncturing.

The proposed SCW structure is compared against the Multiple CodeWords (MCWs) adaptive structure. In the MCWs structure, the transmitter divides the data over different subbands (resource blocks). The data is then encoded, interleaved and modulated separately over individual tiles. Hence, multiple codewords are transmitted over different tiles. In the proposed structure, the data is encoded with the lowest available code rate then the single codeword is divided among the different tiles where it is punctured differently according to the channel quality of the tile. In other words, the puncturing pattern may change within a single codeword for different tiles, thus the puncturing pattern is adaptive. Note that the proposed structure enables us to use longer codewords that may span several consecutive OFDM symbols. This long codeword is punctured adaptively to achieve different rates over the tiles and thereby improve the throughput. The SCW method can be applied for Turbo and Convolutional codes.

Two methods for interleaving the coded bits are proposed. In the first method, data punctured with the same rate is grouped for interleaving then it is modulated on a per-tile basis; we call this method “puncturing dependant interleaving” (PDI). In the second method the coded data is interleaved before it is punctured; we call this method “interleaved puncturing” (IntP).

Loading schemes are used for rate selection. Different loading schemes are investigated in the thesis, and a new loading scheme is proposed for the novel SCW structure. This new loading scheme benefits from the frequency diversity advantage provided by the SCW structure. The performance of the proposed SCW structure is evaluated using different loading schemes, and it is shown that the SCW is superior to the MCWs structure. The gain of the SCW over the MCWs can reach up to 25-50% at small tile sizes.

The thesis is constructed as follows: In Chapter two, a survey for the adaptive transmission is provided. In Chapter three, the proposed system model for rate-adaptive coded OFDMA systems is introduced and the different loading schemes used in the adaptation process are investigated. In Chapter four, simulation results are provided. Finally, the thesis is concluded in Chapter five.

CHAPTER 2
LITERATURE REVIEW

2.1. Adaptive resource allocation

Adaptive transmission is a powerful way for effective communications over time- and/or frequency- varying channels, as it benefits from the good channel conditions when they occur and preserve the robust transmission during deep fades. Various schemes for adapting to the wireless environment by changing the transmission parameters (e.g. modulation order, code rate/scheme, transmission power etc.) have been studied in the literature.

In [1], changing the modulation during transmission according to the channel quality is proposed. In the proposed method a higher modulation orders are chosen at a good channel conditions and a lower orders of modulation are used when the channel conditions degrade. The proposed adaptive modulation scheme is based on the received signal strength (RSSI). It was shown that the proposed scheme provides around 5dB gain over fixed transmission using QAM.

In [2], an uncoded variable rate - obtained by changing the constellation size - variable transmit power adaptive scheme is proposed for single carrier systems. The proposed scheme obtains 5-10dB gain over the variable power fixed rate scheme, and 20dB gain over the non adaptive transmission. The system model used is shown in Figure 2.1. The adaptation problem is defined as:

- Maximize the average throughput
- Constraints:

- fixed total power
- Instantaneous BER does not exceed a predefined target.

The power adaptations methods considered in [2] are:

1. Water filling (optimal method): More power is given to favorable channel gains, and low power is given to the degraded channels.

2. Channel inversion (sub-optimal method): The power is adapted in order to achieve constant received signal to noise ratio. By applying more power to the strongly attenuated channels and less power to the 'good' channels. Thus, larger transmit power is used to compensate deep fades. Using channel inversion method for power control in fading channels, the channel is regarded as AGWN channel to the encoder and the decoder.

3. Truncated channel inversion (sub-optimal method): maintains a constant received SNR unless the channel fading amplitude falls below a given cutoff level. If the fading channel falls below the cutoff level the radio will not transmit. This method does not waste large power to compensate for the deep channel fades.

Continuous rate adaptation, where the rate may take any real value, and discrete rate adaptation, where the rate can only take limited discrete values, are considered in [2]. In the discrete rate adaptation, rate regions are defined such that in each region there is a channel SNR range associated with certain constellation size and power level.

In the considered system model in [2], the receiver obtains the channel information and sends it to the transmitter through feedback channel. The effect of

channel estimation error and the feedback delay on the adaptation process are also studied. The feedback delay has a negative impact on the adaptation process as the radio adapts based on a delayed version of the channel. Also in case of channel estimation errors the transmission parameters will be determined according to a wrong channel estimate. Thus channel estimation errors and feedback delay will influence the adaptation process and increase the overall BER. It has been shown that for a target BER of 10^{-3} the estimation error should be less than 1dB, and less than 0.5dB if the target BER is 10^{-6}.

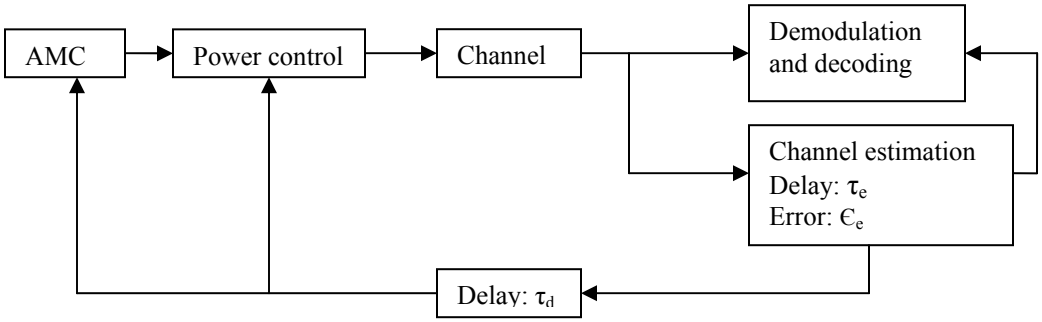

Figure 2.1: System model used in [2] and [3]

Adaptive modulation and coding (AMC) promises yet more gains over the adaptive modulation fixed coding schemes. Adaptive trellis-coded modulation and turbo-coded modulation were studied in [3] and [4] respectively, and it was shown that 3dB gain is obtained by the adaptive turbo-coded modulation over the adaptive eight-state trellis-coded modulation.

In [4], discrete rate adaptive turbo coded modulation is employed in a single carrier system. In the adaptation problem considered, additional turbo code constraint is added to the average power and the BER constraint. The additional turbo constraint ensures that the channel remains unchanged, i.e remains in the same rate region, while the turbo block is being transmitted. Since there is no closed form expression for the BER for the turbo coded modulation system in

AWGN environment, the different power levels that ensure the required BER are obtained using simulations. The system model is the same as in [2] shown in Figure 2.1.

Recent studies have focused on employing ACM in multicarrier orthogonal frequency division multiplexing (OFDM) systems. OFDM is employed by current wireless standards for its robustness to the channel multipath fading. Its tolerance to the inter-symbol interference (ISI) makes high rates transmission over fading channels possible. OFDMA is also considered as the multiple access method for the 4^{th} generation networks.

The 802.16e (WiMAX) standard employs adaptive modulation and coding such that the code rate and the modulation scheme are changed in accordance with the link quality. However, the transmission parameters can be varied for each user on a frame by frame basis [5]. We refer to this adaptation methodology as a per frame adaptation. OFDM system performance is affected by subcarriers experiencing deep fades. Efficient loading of subcarriers is needed to improve the performance in fading channels.

In [6], adaptive transmission is employed in a bit-interleaved coded OFDM system. The adaptation is performed on a per frame basis. The loading scheme used employs BER estimation for each snapshot of the fading channel; based on the estimated BER the rates are determined.

In [7], adaptive modulation over subcarriers is proposed. A significant improvement is achieved compared to fixed transmission OFDM systems.

In [8], a scheme for adaptively loading the carriers under a packet error rate constraint is introduced, where the power and the modulation order are varied over

each subcarrier according to the channel quality. The code rate is also adapted but is invariant over the whole frame and changes from a frame to the other. A significant improvement in the performance is achieved over the uniform rate and power allocation. A per subcarrier adaptation requires precise information about the channel over each subcarrier, this results in a huge feedback overhead to exchange the channel quality between the transmitter and the receiver.

In [9], it is proposed to reduce the overhead introduced from the per subcarrier adaptation by adapting to the wireless environment on a per subband basis, where a subband is a group of contiguous subcarriers. In subband adaptation, all carriers in the same subband use the same transmission parameters while different subbands may be assigned to different transmission parameters based on the channel quality at each subband (tile).

Three allocation algorithms were investigated:

1. Fixed threshold algorithm: In this scheme the SNR thresholds associated with the different modulation orders are tabulated. These thresholds are determined to guarantee certain error performance. The SNR of each subband is compared with the listed thresholds; then the highest modulation order at which the instantaneous SNR of the subband is greater than its corresponding threshold is selected. This scheme assumes a constant instantaneous SNR over each subband, this assumption requires that the coherence bandwidth of the channel be almost equal to or greater than the subband width.

2. Subband BER estimator adaptation algorithm: This scheme supports different SNR values for the different carriers in the subband. An average BER estimator method is used such that the average BER is calculated

using the different modulation schemes. The scheme with the highest throughput and its estimated average BER is lower than the maximum acceptable BER is selected for transmission.

3. Constant throughput adaptive OFDM: This type of adaptation algorithm is suitable for real time audio and video transmission. These applications require a constant data throughput to be transmitted in each time and thus can sacrifice any guaranteed error performance.

In [9], the modulation order is varied from one subband to the other, however, changing the code rate for each subband was not studied. A combined adaptive coding and modulation with the subband loading is introduced in [10] and [11].

In [10], the power, code rate and modulation order are varied according to the channel response in an adaptive OFDM system. The code rate and modulation order are varied on a per subband basis. The paper studies different methods for the power variation. It investigates the performance if the power is varied over each subcarrier individually, over each subband and fixed power allocation. For subcarrier power adaptation, the power is varied using channel inversion such that the received signal power is fixed. It was concluded that variable subband power offers 2dB gain in signal to noise ratio over the fixed power adaptation, however the latter still offers 7dB gain over the non-adaptive turbo coded modulation with reduced overhead. The effect of the number of subbands is also investigated. It was shown that as the number of subbands increases the loading becomes more effective offering higher performance gains.

In [11], adaptive modulation and coding schemes for subband adaptive OFDM systems are investigated. Two different rate selection methods are introduced and

compared, namely the fixed threshold adaptation algorithm and the optimal adaptation algorithm. The two schemes aim at selecting the suitable rates that maximize the throughput while maintaining the error rate performance below a certain predefined value (target BER). The rate selection schemes are described as follows:

1. The fixed threshold adaptation algorithm: Since there are several SNR values in each subband, the choice of the rate in a given subband depends on the worst (lowest) SNR in the subband. In this scheme the worst SNR value is compared with the SNR thresholds of the different rate combinations determining the code rate and modulation order. We term this method as the worst SNR based scheme and it will be further illustrated in chapter 3.

2. The optimal adaptation algorithm: This scheme provides a better trade-off between the throughput and the BER by choosing more suitable rates in each subband according to the channel quality. In this scheme a recursive check on the BER is performed in order to select the highest rate that guarantees the error performance. This scheme is illustrated in details in chapter 3.

2.2. Effective SNR mapping

In addition to the different loading schemes mentioned before, there are other adaptation methods studied in the literature. The first step in most of the adaptation algorithms is the evaluation of the performance metric (ex. PER, BER) from the channel state information (CSI). For example in [6] and [12], the PHY layer adaptation is based on estimating the instantaneous BER.

The performance metric is evaluated according to the link quality, and then the MCS is chosen accordingly. The main difficulty in applying the adaptive modulation and coding schemes (AMC) to multi-carrier systems (OFDM) is the unequal SNR levels in the different subcarriers. Different methods for obtaining a Link Quality Metric (LQM) for multi-carrier systems based on the Effective SNR Mapping (ESM) are present in the literature. The effective SNR based approaches are used to map the channel state information (CSI) of the fading channel, which is a set of the individual subcarriers SNRs, into a single effective SNR value (SNR_{eff}). The effective SNR value represents the fading channel by an equivalent AWGN channel. Using the effective SNR value the estimation of the performance metric, for example the packet error rate (PER), in a fading channel can be obtained using the AWGN simulations such that [13]:

$$PER_{Fading}(\{SNR_1, SNR_2 \ldots SNR_{Nc}\}) = PER_{AWGN}(SNR_{eff}) \qquad (2.1)$$

where SNR_i is the SNR of the i^{th} carrier and N_c is the total number of carriers. The above relation should hold for each instantaneous channel realization.

The effective SNR obtained from the mapping can be used for instantaneous link performance evaluation and link adaptation as shown in Figure 2.2.

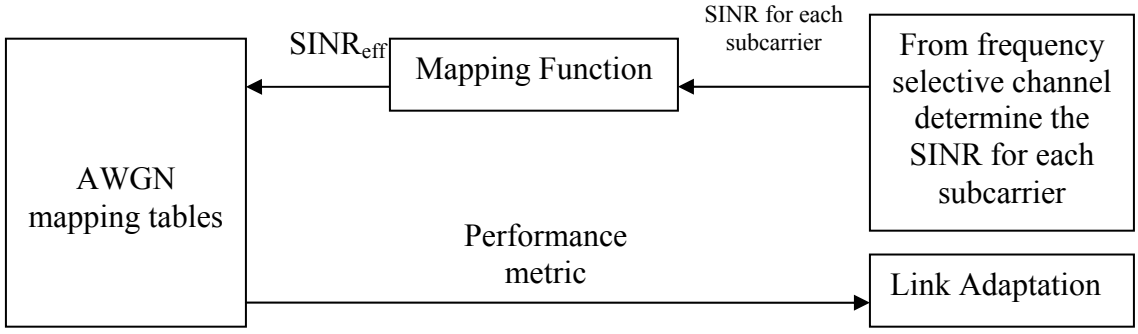

Figure 2.2: Link performance evaluation and link adaptation using ESM

There are different ESM schemes in the literature. Generally, ESM methods can be described as [13]:

$$SNR_{eff} = \phi^{-1}\left\{\frac{1}{N}\sum_{n=1}^{N}\phi(SNR_n)\right\} \qquad (2.2)$$

where $\phi(.)$ is an invertible mapping function.

The different ESM methods apply different mapping function to the individual SNR levels. Three different mapping functions are considered in this chapter. The first is based on the linear average function, the second is based on the exponential mapping function, and the third is based on the mutual information function.

a) Linear average for the instantaneous SNR [14].

The effective SNR is given by

$$SNR_{eff} = \frac{1}{N_c}\sum_{n=1}^{N_c} SNR_n \qquad (2.3)$$

It has been shown in [14] that the instantaneous average SNR is not an accurate LQM.

b) Exponential effective SINR mapping (EESM) [15] [16] [17].

The effective SNR is given by:

$$SINR_{eff} = -\beta \ln\left(\frac{1}{N}\sum_{n=1}^{N} e^{-\frac{SNR_n}{\beta}}\right) \qquad (2.4)$$

The parameter β is an adjustment parameter that depends on the modulation scheme, coding scheme and the encoding block size. This parameter should be

adjusted separately for the different modulation schemes and code rates in order to tune the EESM method and minimize the error in the mapping.

c) Mutual information effective SINR mapping [18] [19].

In the MIESM method no adjusting factor is required for convolutional and turbo codes in contrast to the EESM method that requires adjusting factors for the different modulation and coding schemes. It is easier to apply the MIESM when different modulation schemes are used by the different carriers. It also provides a relatively higher accuracy.

In [20], MIESM is used for fast link adaptation, such that the effective SNR obtained is used to estimate the PER. Then the suitable modulation and coding scheme is accordingly selected. In [13], the MIESM is also used to predict the instantaneous link performance through using the AWGN link tables.

The MIESM approach is considered in this thesis for performance evaluation and link adaptation as will be discussed in more details in chapter 3 and chapter 4.

CHAPTER 3
ADAPTIVE PUNCTURING FOR OFDMA SYSTEMS

3.1 Introduction

The basic idea behind the adaptive modulation and coding (AMC) is to exploit the good environmental conditions to transmit at high data rates by changing the modulation and coding scheme (MCS). Thus, high data rates are used in good channel conditions, and low data rates are used as the channel conditions degrade. This improves the overall system throughput as discussed in the previous chapters. The main contribution of this work is to introduce a novel tile adaptive coded-OFDMA physical layer structure and investigate its performance under different adaptation methodologies. The description of the new system model is provided in this chapter; also different methods for adaptation to the wireless environment are explained.

It is noted that a higher rate codes can be obtained by puncturing lower rate codes. Puncturing a code to obtain higher code rates has the advantage of having the same encoder structure to obtain the different rates. It also has lower complexity since the decoding of unpuntured (n_1,k_1,m_1) code requires 2^k metric computation at each state, however, obtaining (n_1, k_1, m_1) code by puncturing the (n, 1, m), code only two metric computations are required at each state for decoding [21].

In this chapter we introduce changing the MCS for each tile using a novel architecture for rate-adaptive coded OFDMA systems. In our proposed structure, the data for the whole frame is encoded with the lowest available code rate, then

the single codeword (SCW) is divided among the different tiles where it is punctured differently according to the channel quality for each tile. Thus, longer codewords that span several consecutive OFDM symbols are used regardless of the tile size. Two methods for interleaving the coded bits, “puncturing dependant interleaving” (PDI) and “interleaved puncturing” (IntP), are proposed. The new system is compared with the multiple codewords (MCWs) adaptive structure used in [10] and [11], where the transmitter divides the data over different tiles. The data is then encoded, interleaved and modulated separately over individual tiles as shown in Figure 3.1.

The different loading schemes used for constant and variable bit rate applications are presented in this chapter. For variable bit rate adaptive systems, we introduce the worst SNR based scheme, the recursive scheme which is based on the average BER, the Mutual information effective SNR mapping which is based on the effective SNR, maximum goodput scheme, and finally the proposed recursive MIESM scheme.

This chapter is organized as follows: In section 3.2, the proposed adaptive system model is introduced for convolutional and Turbo codes; the different loading schemes are presented in section 3.3. Practical consideration in the adaptive systems is introduced in section 3.4.

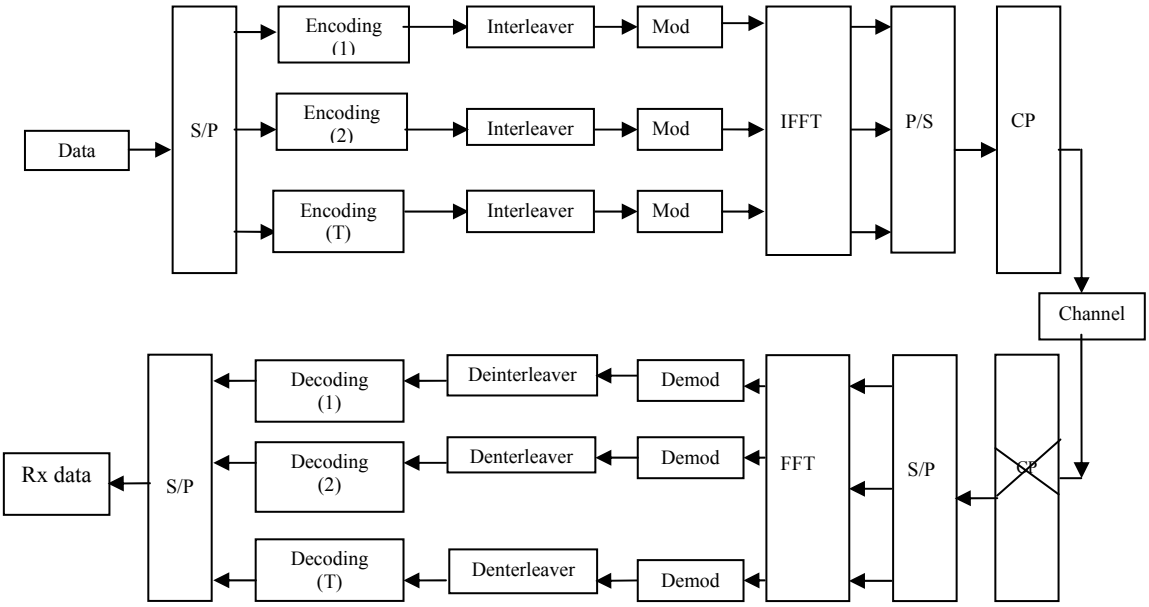

Figure 3.1: MCWs structure.

3.2 System Model

3.2.1 Adaptive Punctured Convolutional Codes

Zone loading of the rate adaptive coded OFDMA systems can be performed by having a single long codeword and then adaptively puncturing this codeword to produce different transmission rates over the tiles. The proposed system structures can be applied to convolutionally coded system as shown in Figures 3.2 and 3.3, assuming that there are *M* available code rates (R_1, R_2 ... R_M), and the OFDM frame is divided into *T* tiles [22]. In the first proposed structure the transmitter encodes the data using the lowest rate convolutional encoder. The coded bits are then divided into *T* groups where it is punctured, interleaved and modulated, then IFFT (inverse fast Fourier transform) is applied followed by cyclic prefix insertion.

Interleaving in rate adaptive coded OFDMA systems must not allow coded bits with a certain rate to be mapped to a tile that should be loaded with another rate. This was previously achieved by using per-tile interleaving (PTI), where the coded bits on each tile are interleaved separately [10-11]. However this limits the interleaver size to the tile size. This restriction is reduced in the PDI and completely removed in the IntP structure as will be illustrated.

In the PDI structure we have M interleavers, one for each rate, as shown in Figure 3.2. After interleaving, the bits are mapped to the correct tiles, such that if tile t (where $t \in \{1,2,\cdots T\}$), according to the adaptive scheme should be loaded using rate R_i (where $i \in \{1,2,\cdots M\}$), then after interleaving that tile is still loaded with bits that are encoded with the same rate (R_i).

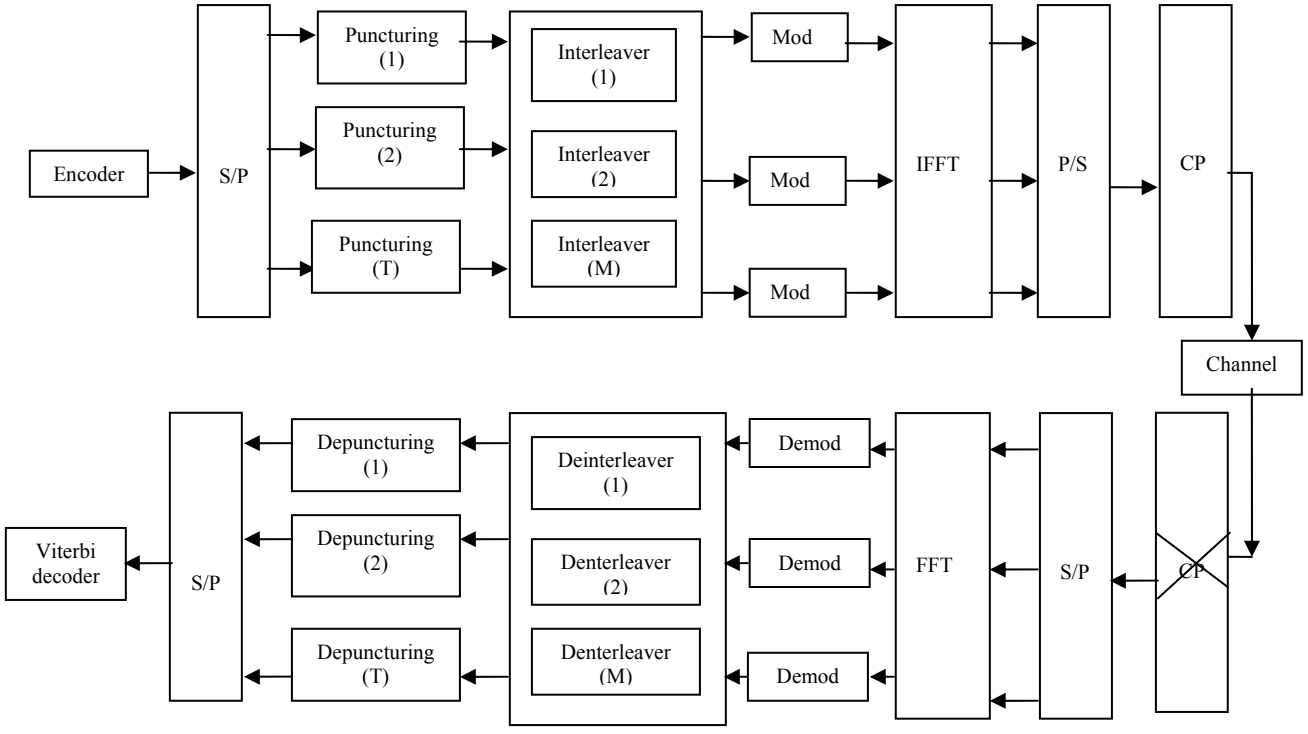

Figure 3.2: The Proposed SCW-PDI structure.

In the second proposed IntP structure, the interleaving is performed prior to puncturing as shown in Figure 3.3. In this case the interleaver size depends on the codeword length and is independent of the tile size. Note that interleaving in this manner is unconventional since the interleaver is virtually embedded in the encoder if one is to view the encoding and puncturing as one effective encoding operation. One problem this may present is that the deinterleaver at the receiver will upset the depuncturing pattern, possibly resulting in bursts of depunctured bits at the decoder input. Applying a deinterleaved puncturing pattern at the transmitter is not a remedy since this will disturb the original tile-adaptive puncturing. Joint interleaving and puncturing patterns may be designed to alleviate this potential problem. In this structure we use interleaving pattern that forces the depunctured bits at the decoder input to be uniformly spread over the codeword. More sophisticated interleaving patterns could be employed to further improve the performance. This would be a subject of future research.

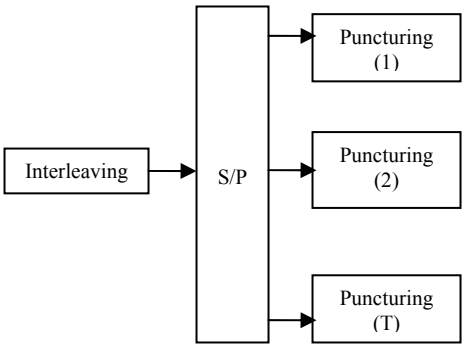

Figure 3.3: Interleaved puncturing (IntP).

At the receiver the inverse operation is performed; the cyclic prefix is removed, FFT is applied then the frame is demodulated, deinterleaved and depunctured, then decoded. The depuncturing process is done by inserting zeros at the same locations of the punctured bits.

The MCWs structure used in adaptive coded OFDMA systems employs separate coding and puncturing processes on each tile to obtain the required rate. It is shown via simulations that our proposed SCW structure is superior to the MCWs structure especially at small tile sizes.

3.2.2 Adaptive Punctured Turbo Codes

The proposed adaptive puncturing scheme is applied to the double binary convolutional turbo codes (CTC) defined in the WiMAX standard (802.16e) [23]. The encoder is termed as double binary as it processes two input bits at the same time. The encoder is systematic such that the first two encoder outputs are the input bits. In the next subsections, the description of CTC encoding procedure is provided, followed by the system model of the adaptive puncturing technique using CTC.

3.2.2.1 CTC description

3.2.2.1.1 Constituent encoders

The CTC encoder considered is shown in Figure 3.4. The mother code rate is 1/3. The constituent encoders have a constraint length of four. The polynomials that define the connections of each encoder are:

- For Feedback branch: $1+D+D^3$
- For Y parity: $1+D^2+D^3$
- For W parity: $1+D^3$

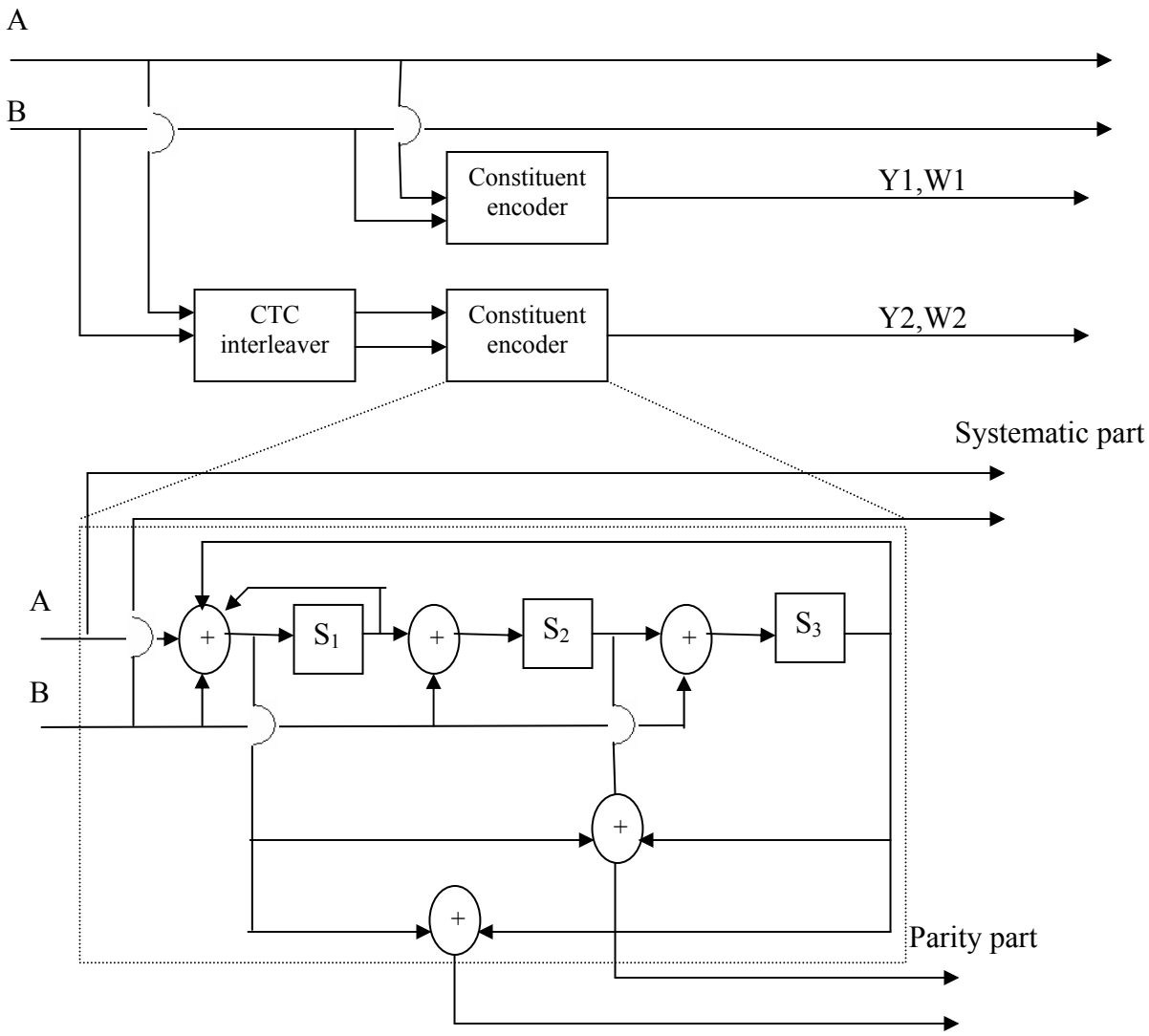

Figure 3.4: CTC encoder

The block size input to the CTC encoder is denoted by N; N_{EP} is number of information bits input to the CTC encoder, such that, $N_{EP} = 2N$.

3.2.2.1.2 CTC interleaver

The CTC interleaver specified by the WiMAX standard 802.16e [23] consists of two interleaving steps. The first is on the symbol level, and the second is on the block level.

Step1: Switch alternate couples

This step is described as follows:

For i=1:N
If (j mod 2 == 0) Let (A,B)=(B,A)

If the input to this stage is $[(A_0,B_0), (A_1,B_1), (A_2,B_2),...., (A_{N-1},B_{N-1})]$, then the output of this stage is $O1=[(A_0,B_0), (B1_1,A1_1), (A_2,B_2),...., (B_{N-1},A_{N-1})]$.

Step2: block level interleaving

The function $P_i(j)$ provides an interleaved address of the j^{th} couple or symbol, such that:

for $j = 0:N-1$
switch $j \bmod 4$:
Case 0:
$P(j) = (P0.j+1) \bmod N$
Case 1:
$P(j) = (P0.j+1+N/2+P1) \bmod N$
Case 2:
$P(j) = (P0.j+1+P2) \bmod N$
Case 3:
$P(j) = (P0.j+1+N/2+P3) \bmod N$

Where P0, P1, P2, P3 are interleaving parameters specified by the standard [23] and are dependent on the block size *N*.

3.2.2.1.3 Circulation states

Unlike the convolutional codes that can be terminated by appending zeros at the end of the data sequence to reach to all zero state. Turbo codes are not terminated by appending zeros, as this will not ensure that the two constituent encoders will be terminated. Also, due to the recursive structure of the encoders, appending zeros to the data sequence does not ensure terminating the trellis. Instead, a state is determined for each encoder such that if the encoder starts at this state it will also end at the same state. This state is called the circulation state (*Sc*). The circulation state depends on the block size. To obtain the circulation state the following steps are followed:

1. States are initialized to zero for both encoders.
2. The data is encoded and the final state reached at each encoder $(S0_{N-1})$ is used to determine its circulation state using the Table 3.1.

Table 3.1: Determination of circulation state

$Nmod_7$	$S0_{N-1}$							
	0	1	2	3	4	5	6	7
1	0	6	4	2	7	1	3	5
2	0	3	7	4	5	6	2	1
3	0	5	3	6	2	7	1	4
4	0	4	1	5	6	2	7	3
5	0	2	5	7	1	3	4	6
6	0	7	6	1	3	4	5	2

3.2.2.1.4 Subpacket generation

The output of the CTC encoder is interleaved then punctured to produce subpackets with different coding rates. The following operations are performed for subpacket generation:

a. Symbol separation
b. Subblock interleaving
c. Symbol grouping
d. Symbol selection (Puncturing)

The subpacket generation steps are shown in Figure 3.5.

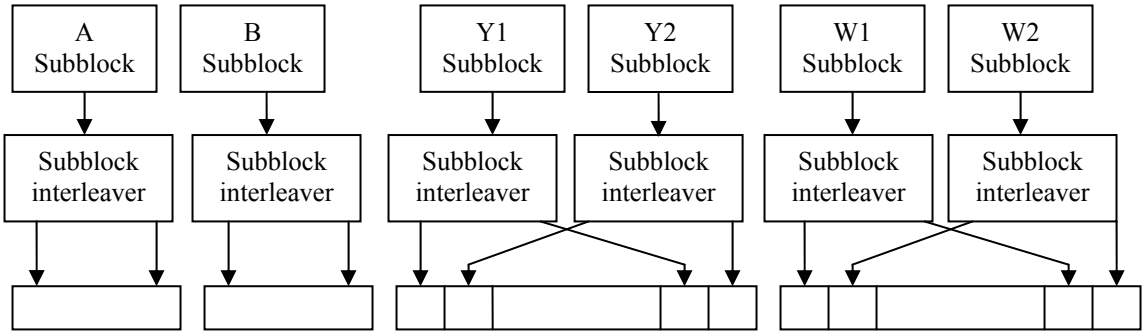

Figure 3.5: Symbol separation, subblock interleaving, and symbol grouping

a. Symbol separation

The encoder output is demultiplexed into six subblocks. Two systematic sublocks denoted by *A* and *B*, and four parity subblocks denoted by *Y1, Y2, W1* and *W2*. The size of each subblock is *N* (bits).

b. Subblock interleaving

This is a mandatory step for puncturing, since puncturing is performed by erasing consecutive symbols. These consecutive symbols should by an interleaved version of non consecutive bit positions. Each subblock is interleaved separately. The subblock to be interleaved is written into an array at addresses from 0 to *(N-1)*; after interleaving the i^{th} symbol in the subblock is mapped to an address AD_i. The interleaving procedure is described as follows:

1. Depending on the block size the interleaving parameters *(m, J)* are determined from Table 3.2.
2. Counters *i* and *K* are initialized to zero
3. Tentative output address T_k is formed according to the formula

$$T_k = 2^m (K \bmod J) + BRO\left(floor\left(\frac{K}{J} \right) \right) \qquad (3.1)$$

Where $BRO_m(y)$ is the bit-reversed *m* bit value of *y* (i.e., $BRO_3(6)=3$).

4. If T_k is less than *N*, then $AD_i = T_k$, and the counters *i* and *k* are incremented by 1. Otherwise discard T_k and increamed *K* only.
5. Process is repeated until the *N* interleaved output addresses are obtained.

Table 3.2: Subblock interleaving parameters

N_{EP}	N	m	J
48	24	3	3
72	36	4	3
96	48	4	3
144	72	5	3
192	96	5	3
216	108	6	3

240	120	6	2
288	144	6	3
384	192	6	3
432	216	6	4
480	240	7	2
960	480	8	2
1920	960	9	2
2880	1440	9	3
3840	1920	10	2
4800	2400	10	3

c. Symbol grouping

The output block of the symbol grouping consists of *A* subblock, *B* subblock, a symbol by symbol multiplexed block of *Y1* and *Y2* and finally a symbol by symbol multiplexed block of *W1* and *W2*.

d. Symbol selection (puncturing)

In order to obtain different transmissions rates, symbol selection (puncturing) is applied to the output block of the symbol grouping. Puncturing is performed by the erasure of consecutive bits or equivalently selecting consecutive bits to be transmitted.

The punctured output (subpacket) contains the symbols with indices that starts from $(F_k) mod_{6N}$ to $(F_k + 2N/code\_rate - 1) mod_{6N}$ as shown in Figure 3.6. The term F_k represents an offset from the beginning of the input block

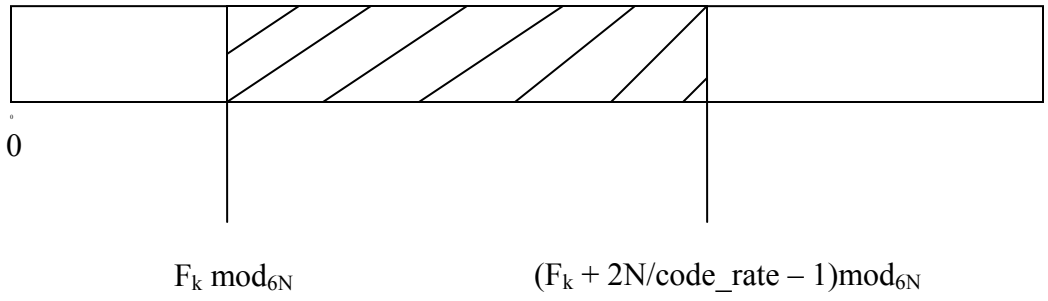

Figure 3.6: Symbol selection (Puncturing process)

The i^{th} symbol in the K^{th} punctured subpacket is at the index $S_{K,i}$ in the original packet, such that:

$$S_{K,i} = (F_K + i) \bmod (3N_{EP}) \qquad (3.2)$$

For the non HARQ applications, F_k is equal to zero and the above expression can be written as:

$$S_i = i \bmod (3N_{EP}) \qquad (3.3)$$

such that $i = 0,1,2,.....,L_k - 1$, where L_k is the length of the final codeword and can be expressed as:

$$L_k = \frac{2N}{code\_rate}. \qquad (3.4)$$

The above equations show that for non-HARQ applications the puncturing process is obtained by selecting the first $\frac{2N}{code\_rate}$ bits from the input to the puncturing block.

3.2.2.2 Adaptive coding

3.2.2.2.1 Per-Frame Adaptation (PFA)

In the PFA the transmission parameters are varied on a per frame basis. Thus, the rate of each frame varies according to the channel conditions, consequently the turbo block size changes. The frame may be divided into more than one block depending on the frame size and supportable block sizes by the standard. Each block is encoded using the CTC encoder and punctured by the same manner discussed earlier to obtain the required rate. For tile based adaptation where the code rate changes from one tile to the other in the same frame, MCWs and SCW can be applied.

3.2.2.2.2 MCWs

For the MCWs, shown in Figure 3.7, the frame is divided into tiles. Each tile is encoded with the CTC encoder and punctured by the same manner discussed before. The number of bits loaded on each tile depends on the tile size and its assigned rate combination. The input to the tile may be sub-divided into blocks depending on the supportable block sizes by the standard; each block is then encoded separately.

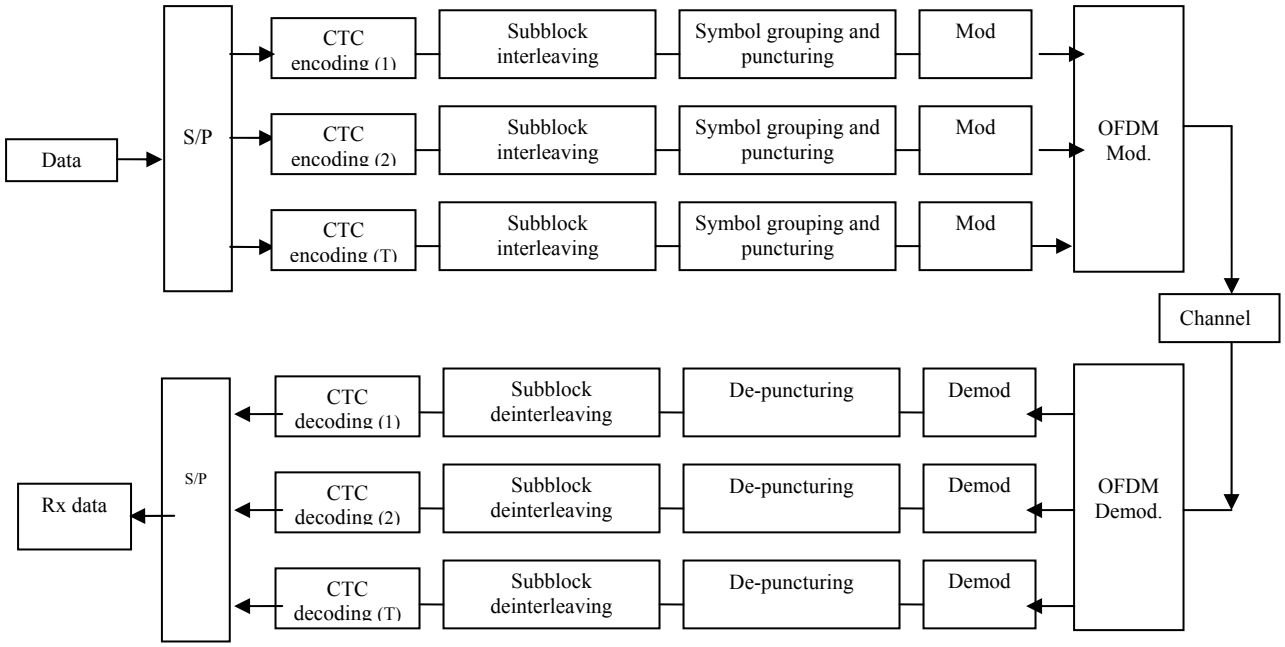

Figure 3.7: The structure of MCWs using Turbo codes

3.2.2.2.3 SCW

In the SCW structure, the whole frame is encoded with the mother code rate which is rate 1/3 in the mentioned CTC encoder. Then the coded blocks are divided into groups, each group is punctured with the same rate. The size of each group depends on the number of tiles that are assigned to the same code rate and the number of information bits that should be loaded on each tile, which is a function of the tile size and the assigned rate. Each group has an input consisting of six tile-subblocks, two systematic tile-subblocks (say A_1, B_1) and four parity tile-subblocks (say $Y1_1$,$Y2_1$, $W1_1$, $W2_1$). The tile-sublocks are generated from the original subblocks *(A,B,Y1,Y2,W1,W2)* as shown in Figure 3.8. The size of each tile-subblock is $N^{'}$ bits. Such that, if $InpB_t$ is the number of information bits loaded over tile *t,* then $N^{'}$ is given by:

$$N^{'} = \frac{3 * InpB}{6} \qquad (3.5)$$

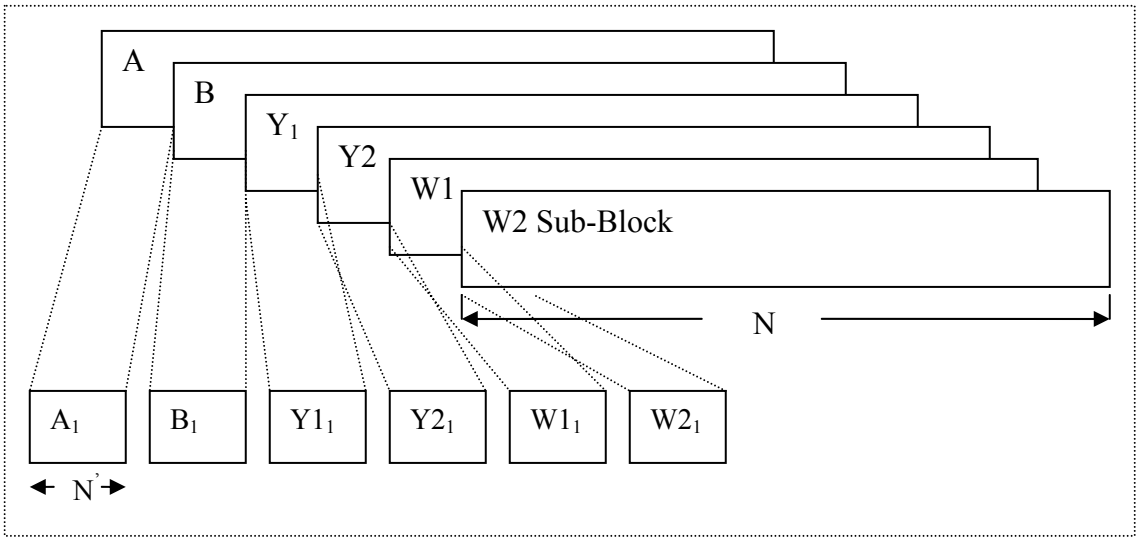

Figure 3.8: tile-subblock generation from the original subblocks

The subblock interleaving, symbol grouping and symbol selection are performed on each group separately. Since the size of the each tile-subbock ($N^{'}$) might not be equal to any of the mentioned block sizes in the standard, there are few modifications needed in the subblock interleaving and symbol selection.

1. For the subblock interleaver, since the length of its input might be a value not considered in Table 3.1. The interleaving parameters (J and m) are determined according to the size of the tile-subblock ($N^{'}$), as follows:

   A. First, J is determined from table 3.3.
   B. Then, m is determined according to the following relation:

$$m = \log_2\left(floor\left(\frac{N^{'} - 1}{J} \right) \right) \qquad (3.6)$$

Table 3.3: Modified Interleaving parameter for SCW

Size of the tile-subblock ($N^{'}$)	J
240	2
480	2
960	2
1920	2
216	4
Otherwise	3

After determining m and J, the same steps for the subblock interleaving in section 3.2.2.1.4 are applied.

2. For puncturing, the only change from the steps in section 3.2.2.1.4 is that N will be replaced by $N^{'}$.

The SCW structure is shown in Figure 3.9.

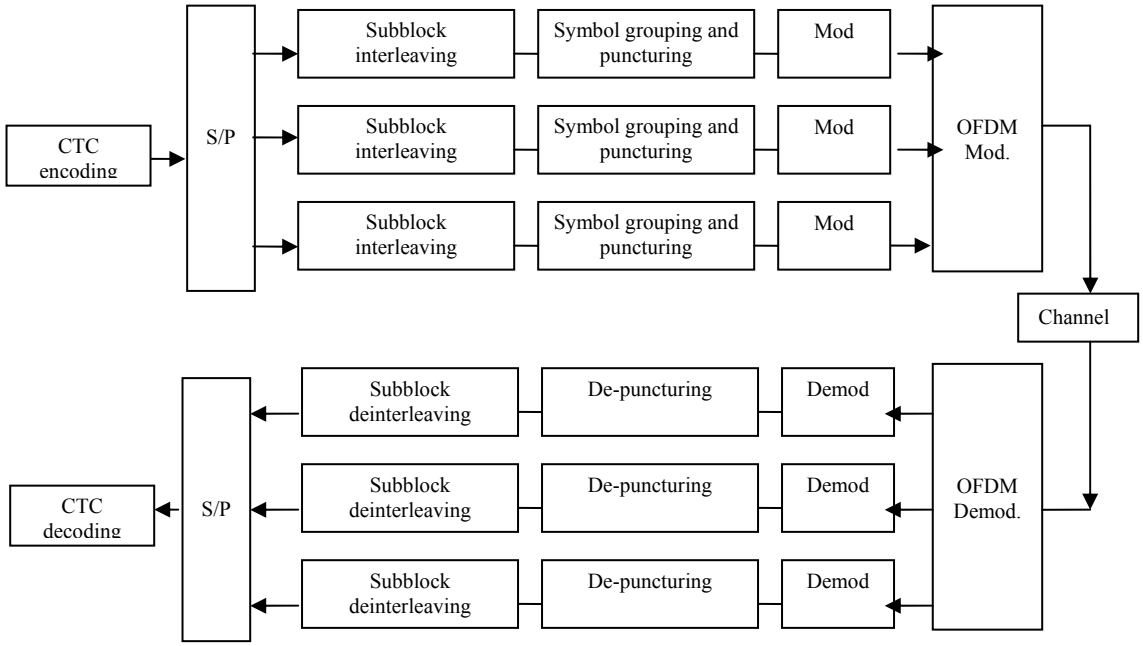

Figure 3.9: The structure of SCW using Turbo codes

3.3. Adaptive loading

Adaptive loading schemes select the suitable transmission parameters according to the channel quality. When zone loading is employed, the MCS may change from one tile to the other in the same OFDM frame. Thus, the loading scheme selects the suitable rate for each tile; also in the PFA the transmission parameters for each frame is obtained. A channel evaluation criterion must be present in order to select the suitable transmission parameters in a fading environment. In this section we will discuss the worst SNR based scheme, the average BER based scheme, which we term as the recursive scheme, and the effective SNR scheme based on mutual information effective SNR mapping (MIESM). A new scheme is also proposed for the SCW structure, termed as recursive MIESM (R-MIESM). The new scheme exploits the frequency diversity advantage that the SCW provides. The frequency diversity is obtained from the fact that in decoding a single codeword, the "good" channel conditions over some tiles may compensate the errors occurred in faded subcarriers. This advantage is not present in the MCWs structure since each tile is separately encoded and decoded.

All the adaptation schemes use SNR thresholds to determine the suitable rate combination (code rate and modulation order pair) for transmission. Switching SNR thresholds are determined from the AWGN simulations based on the required error performance. These thresholds guarantee that a certain target BER (BER_{target}) is not exceeded.

3.3.1. Worst SNR based scheme

The different carriers in the same tile have different signal-to-noise ratios depending on the fading channel frequency response. If h_n is the channel response at the n^{th} carrier, then the modified SNR of carrier n is given by:

$$SNR_n = | h_n |^2 \; SNR \qquad (3.7)$$

In this scheme the worst SNR in each tile is compared with the SNR thresholds that guarantee the BER_{target}. Then the highest rate combination such that its threshold is less than the worst SNR, is selected for transmission [11]. Since this scheme relies on the worst SNR in each tile, the BER performance is normally less than BER_{target}. Using more representative channel quality measurement, higher rates can be used without exceeding the target BER.

3.3.2. Recursive scheme

The recursive scheme is used to determine the transmission rates according to the channel and the target BER. It employs a recursive check on the BER performance to select higher rates as will be illustrated in the following steps:

a. For each tile, the rate combination based on the worst SNR in the tile is determined (assume that the rate combination is at index α in the look-up table that lists the available rates).

b. For the next higher rate (at index α+1), the BER of each carrier in the tile is obtained from the non adaptive AWGN curves and by using the modified SNRs of the carriers. Then, the average BER of the tile is computed.

c. If the average BER obtained from the curves is still below the target error rate (BER_{target}), a higher rate is selected (at index α+2) and the average BER is re-calculated for the tile and compared with the target BER. The process is repeated until the average BER exceeds BER_{target} and the last rate combination that satisfied the target BER is assigned to the tile.

Note that if the minimum SNR in the tile is below the lowest threshold, the tile is not used for transmission and no further checks are done on the BER.
This scheme is referred to as the optimal adaptation algorithm in [11]. The flow chart of the recursive scheme is shown in Figure 3.10.

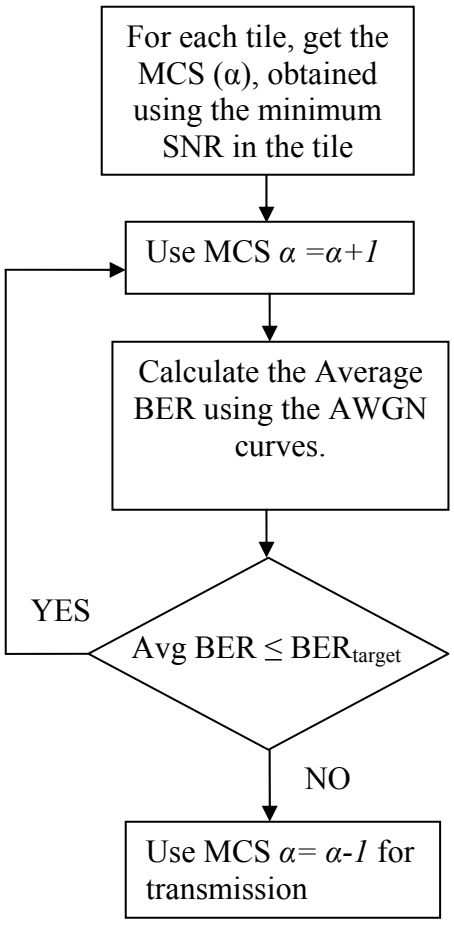

Figure 3.10: Flow chart of the recursive scheme

3.3.3. MIESM rate selection scheme

MIESM mapping scheme is outperforming the other mapping methods (ex. EESM) [19]. Using the MIESM, the SNR values of the subcarriers in each tile are mapped to a single effective SNR value using the mutual information function. The effective SNR obtained from the mapping function is used to predict the instantaneous system performance using the AWGN link tables [15]; in MIESM rate selection scheme the obtained SNR effective is used for link adaptation.

In this section we first derive the mutual information function used for effective SNR mapping, and then we illustrate how we use the obtained effective SNR in the link adaptation.

Derivation of Mutual Information function

Assuming AWGN environment, the received signal y is given by:

$$y = x_m + u \qquad (3.8)$$

where x_m is the transmitted symbol, and u is zero mean complex Gaussian noise with variance σ^2 *(σ^2=No/2=Es/(2 SNR)=1/(2SNR)),* where E_s is the energy per symbol which is normalized to unity.

The symbol mutual information (*SI*) is expressed as:

$$SI = \sum_{m=1}^{M} \int_{y} P(y/x_m) P(x_m) \log_2 \frac{P(y/x_m)}{P(y)} dy \qquad (3.9)$$

where M is the number of constellation points. The prior probability of x_m is $P(x_m)$ and is set to $1/M$. The conditional probability of y given x_m ($P(y/ x_m)$) and the unconditioned probability of y ($P(y)$) are expressed as follows:

$$P(y/x_m) = \frac{1}{\sqrt{2\pi\sigma^2}} \exp\left(-\frac{(y-x_m)^2}{2\sigma^2}\right) \qquad (3.10)$$

$$P(y) = \sum_{k=1}^{M} P(x_k, y) = \sum_{k=1}^{M} P(y/x_k) P(x_k) \qquad (3.11)$$

$$P(y) = \frac{1}{M} \sum_{k=1}^{M} P(y/x_k) \qquad (3.12)$$

$$P(y) = \frac{1}{M} \sum_{k=1}^{M} \frac{1}{\sqrt{2\pi\sigma^2}} \exp\left(-\frac{(y-x_k)^2}{2\sigma^2}\right) \qquad (3.13)$$

Thus the SI can be expressed as:

$$SI = \sum_{m=1}^{M} \int_{y} \frac{1}{\sqrt{2\pi\sigma^2}} \exp\left(-\frac{(y-x_m)^2}{2\sigma^2}\right) \frac{1}{M} \log_2 \left(\frac{\frac{1}{\sqrt{2\pi\sigma^2}} \exp\left(-\frac{(y-x_m)^2}{2\sigma^2}\right)}{\frac{1}{M} \frac{1}{\sqrt{2\pi\sigma^2}} \sum_{k=1}^{M} \exp\left(-\frac{(y-x_k)^2}{2\sigma^2}\right)} \right) \qquad (3.14)$$

By making the above expression as a function of u instead of y, we substitute every y by $y = x_m + u$, we obtain,

$$SI = \sum_{m=1}^{M} \int_{u} \frac{1}{\sqrt{2\pi\sigma^2}} \exp\left(-\frac{u^2}{2\sigma^2}\right) \frac{1}{M} \log_2 \left(\frac{\exp\left(-\frac{u^2}{2\sigma^2}\right)}{\frac{1}{M}\sum_{k=1}^{M} \exp\left(-\frac{(x_m + u - x_k)^2}{2\sigma^2}\right)} \right) \tag{3.15}$$

$$SI = \log_2 M - \frac{1}{M} \sum_{m=1}^{M} E_u \left(\log_2 \left(\sum_{k=1}^{M} \exp\left(-\frac{(x_m + u - x_k)^2 - (u)^2}{2\sigma^2}\right)\right)\right) \tag{3.16}$$

$$SI(SNR, M) = \log_2 M - \frac{1}{M} \sum_{m=1}^{M} E_u \left(\log_2 \left(1 + \sum_{k=1, k\neq m}^{M} \exp\left(-\frac{(x_m - x_k + u)^2 - (u)^2}{(1/SNR)}\right)\right)\right) \tag{3.17}$$

where E_u is the expected value over the AWGN noise.

Computation of mutual information per coded bit, which is termed as Received Bit mutual Information Rate (RBIR), can be obtained from the received symbol mutual information by dividing by the number of bits per symbol, such that:

$$RBIR = \frac{SI(SNR, M)}{\log_2(M)} \tag{3.18}$$

The *SI* curves are generated once for each modulation order, and the *RBIR* values are obtained accordingly. The *SI* and *RBIR* curves are shown in Figure 3.11 and Figure 3.12 for QPSK and 16QAM modulation. The *SI* values are stored in tables in [15] for the different modulation schemes; this table is directly used to obtain the *SI* values.

If N_c subcarriers are used for transmission, the RBIR is computed by dividing by the codeword length as follows [15]:

$$RBIR = \frac{\sum_{n=1}^{N_c} SI(SNR_n, M(n))}{\sum_{n=1}^{N_c} \log_2(M(n))} \qquad (3.19)$$

where $log_2(M(n))$ is the number of bits per transmitted symbol on the n^{th} subcarrier.

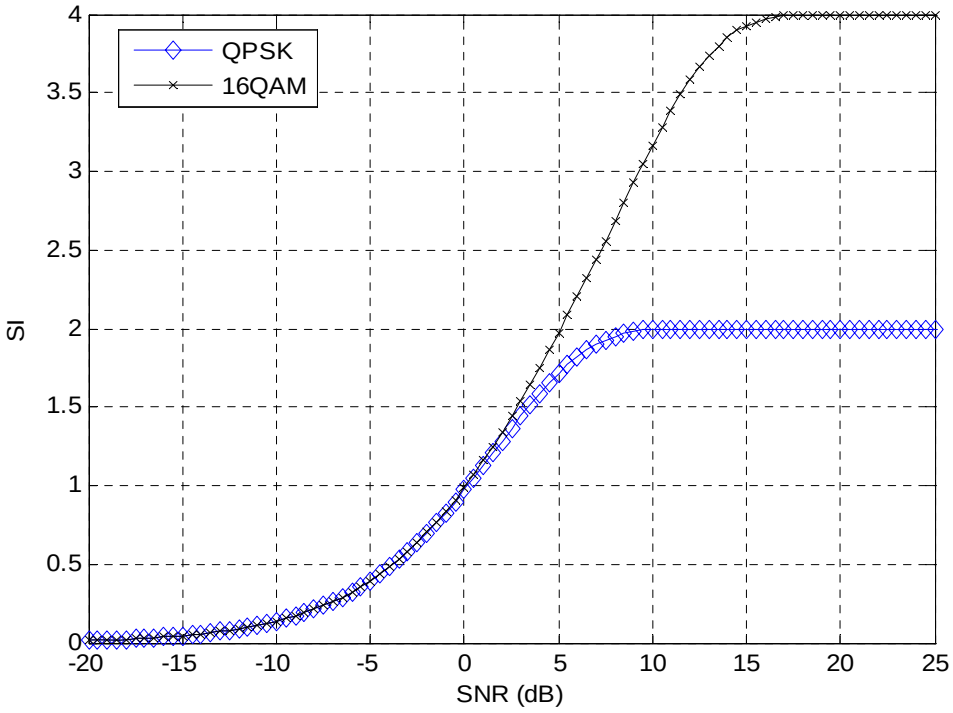

Figure 3.11: SI Vs SNR for QPSK and 16QAM.

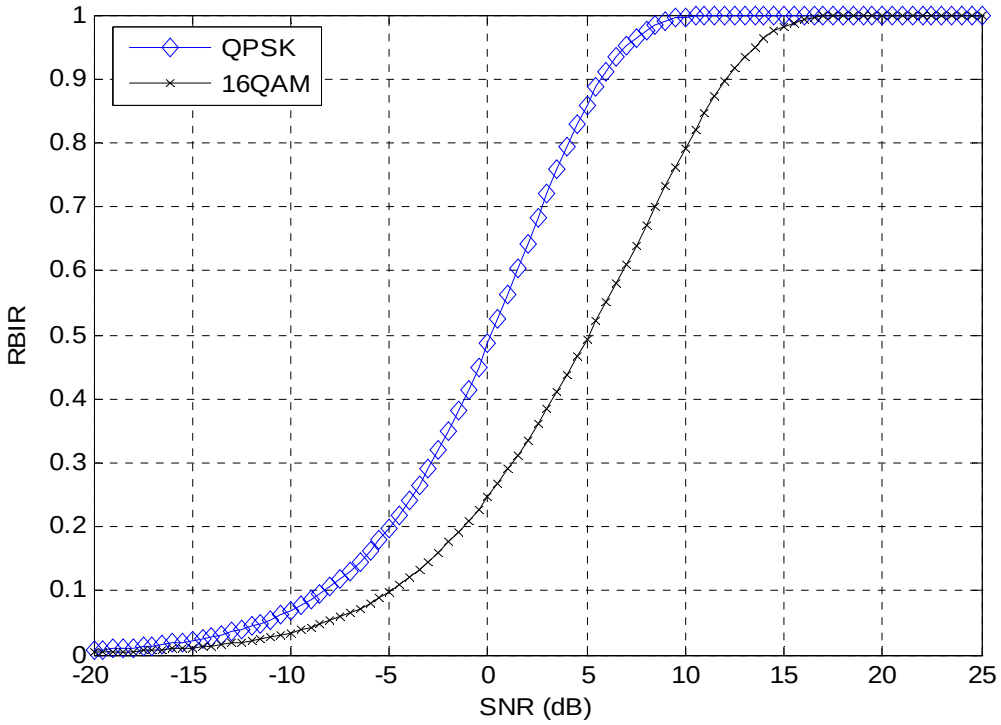

Figure 3.12: RBIR Vs SNR for QPSK and 16QAM.

MIESM adaptive scheme

The MIESM scheme works as follows:

a. For each tile, *SI* values are obtained assuming both QPSK and 16QAM mapping.

b. *RBIR* is calculated for each tile, using equation (3.19). Two values will be obtained, one for QPSK and the other for 16QAM.

c. SNR_{eff} is obtained from the *RBIR* curve, shown in Figure 3.12, for the two modulation schemes using the obtained *RBIR* values.

d. The SNR_{eff} obtained for the 16QAM, is compared with the 16QAM thresholds, and the code rate is determined accordingly.

e. If SNR_{eff} obtained for the 16QAM is less than the lowest 16QAM threshold value (which is the threshold that maintains the target BER using 16QAM and rate ½ code), then the SNR_{eff} for the QPSK is compared with the QPSK thresholds, and the code rate is determined accordingly.

f. If SNR_{eff} of a tile is less than the lowest threshold then this tile is not used for transmission.

If some tiles are not used for transmission, the power is redistributed equally over the other tiles in order to have fixed power for each transmitted frame. Then the above steps are repeated to obtain the new rate assignment based on the modified power levels over the tiles. In this scheme, the SNR_{eff} for any tile can only improve in the second step. Hence, all tiles that pass the first step will be used for transmission. This simple two-step rate selection allows a fair comparison with PFA on an equal transmitted power basis. However, it should be noted that better rate selection may be possible.

3.3.4. Recursive MIESM scheme (R-MIESM)

The single codeword benefits from frequency diversity, such that in decoding a single codeword, the "good" channel conditions over some tiles may compensate the errors occurred in other faded tiles in the frame. We aim at finding a rate selection scheme that makes use of this advantage. We propose a recursive MIESM scheme. The RMIESM rate selection scheme works as follows:

a. The code rate and the modulation order of each tile are determined according to MIESM method described earlier.

a. The BER of each tile is obtained using the effective SNRs of the tiles and the AWGN curves. Using the obtained BER values the average BER of the whole frame is calculated as follows:

$$BER_{avg} = \frac{\sum_{i=1}^{T} Z_i \times BER_i}{\sum_{i=1}^{T} Z_i} \qquad (3.20)$$

such that BER_i and Z_i are the BER and the number of information bits of the i^{th} tile, respectively.

b. If the average BER of the frame does not exceed the target BER, the tile that has the best error performance (lowest BER) is assigned to a higher rate combination. Then steps 2 and 3 are repeated using the new rate assignment.

c. If the average BER of the frame exceeds the target BER, the highest rate assignment that did not exceed the target BER is used for transmission.

We study the R-MIESM methodology with the SCW. It is worth noting that the R-MIESM technique can, in principle, be extended to the MCW systems as well.

3.3.5. Maximum Goodput scheme (Max GP)

The maximum goodput scheme works as follows:

a. The PER is computed for each tile using the AWGN curves of the PER and the effective SNR obtained via the mutual information function. Each tile has a PER value for each MCS denoted by PER_α, where α is the index to the MCS.

b. The goodput of each tile is then obtained for each MCS (GP_α). The goodput is defined as the total number of information bits that is received correctly. It is computed for each tile for all possible values of α as follows [24]:

$$GP_\alpha = (1 - PER_\alpha) I_\alpha \qquad (3.21)$$

where I_α is the number of information bits in the tile if the MCS at index α is used.

c. The MCS that corresponds to the maximum calculated goodput is selected for the tile.

It is noted that the maximum goodput scheme may not achieve the best performance since there is no quality constraint guaranteed. In our simulation for variable bit rate adaptive systems, we focus on the recursive, MIESM and R-MIESM schemes. The simulation results of the maximum goodput scheme are found in the Appendix.

3.3.6. Constant Bit Rate scheme (CBR)

The adaptive schemes discussed above result in variable bit rate transmission, such that the number of information bits in each frame varies according to the channel conditions. This is not applicable in some applications (e.g. speech and video applications) that do not support delays and require fixed data payload to be transmitted in each frame. A constant bit rate adaptive scheme

is used to provide robust fixed data rate transmission. The CBR scheme we use in this thesis assumes having fixed modulation (QPSK) and some available code rates. We assume that if the code rates are evenly assigned over the tiles we reach to the required number of transmitted bits. The code rates are assigned evenly such that a high code rate is assigned to the group of the tiles with the highest average SNR value and low code rates are assigned to the tiles with the lowest average SNR.

It is noted that in the CBR applications, no error rate performance is guaranteed since a fixed data payload is transmitted regardless of the channel quality.

3.4. Practical considerations

In this section we mention two issues that should be considered in practical adaptive systems. The first is the effect of imperfect channel estimation and prediction, and the second is the feedback overhead required for transmission parameters synchronization.

A. Channel estimation and prediction errors

For proper detection of the transmitted frame, channel estimation is required at the receiver side. The channel estimate value is also used for adaptation purposes at the transmitter. In order to adapt to the time varying environment the transmitter not only needs to know the current channel but it uses the current channel value to predict the channel for the next transmission. Thus, channel prediction is also required for a complete adaptive system. Any error in the channel estimation and/or prediction will definitely affect the performance, since this will let the radio adapts to wrong environmental conditions. However, in our

simulations, presented in the next chapter, we assume perfect channel knowledge and we focus on evaluating the performance of the proposed model.

B. Overhead for transmission parameters synchronization

The transmitter and the receiver must agree on the transmission parameters used for proper decoding of the frames. This could be accomplished using a feedback channel. It is required to minimize the feedback overhead. One possible way to do this is to have the receiver doing the channel estimation, predicts the channel in the next transmission interval, and by a certain rate selection criterion the receiver decides the proper rates for the next transmission as shown in Figure 3.13.

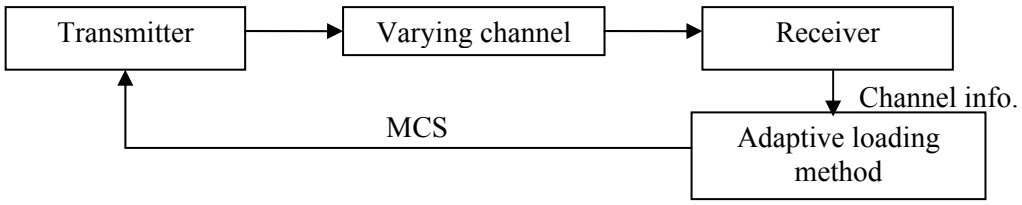

Figure 3.13: Brief diagram for the adaptive system

The receiver needs only to feedback to the transmitter the index to the look-up table that corresponds to the selected rate. Thus, for L available rate combinations and T tiles the total feedback overhead is $T.ceil(log_2(L))$. In case of adapting on a frame by frame basis (PFA), the overhead will be $ceil(log_2(L))$ [5].

CHAPTER 4
SIMULATION RESULTS

4.1 Introduction

In this chapter the performance of the proposed adaptive puncturing technique is investigated under constant bit rate and variable bit rate adaptive schemes. Recursive, MIESM and R-MIESM approaches are employed to obtain variable bit rate adaptive system. In the simulations we compare zone loading, using both MCWs and our proposed SCW schemes, and both are compared against the Per-Frame Adaptation (PFA) where any frame is transmitted using the same transmission parameters over all active subcarriers. It is shown that MIESM based scheme results in a better goodput performance compared to the recursive scheme. Under the different adaptation methodologies, it is shown that the SCW is superior to the PFA and to the MCWs.

Although the adaptation techniques greatly depend on the channel information, in our simulations we assume perfect channel knowledge at the transmitter and the receiver and focus on the structure of the PHY layer rather than the channel estimation and prediction scheme.

This chapter is organized as follows: first the analytical bounds for the punctured convolutional codes are derived in section 4.2; these bounds are used to later estimate the goodput of the SCW and MCWs structures. In section 4.3, the channel model used is described. In sections 4.4 and 4.5 the performance of the SCW is investigated for convolutional and turbo codes respectively.

4.2 Analytical bounds for punctured convolutional codes

In order to have a reliable communication over wireless channels redundancy is introduced by means of channel coding. Convolutional codes are a known class of channel coding used for robust transmission over wireless channels and it is the mandatory error correcting code in some wireless standards (e.g. WIMAX standard 802.16e) [23]. The performance analysis of convolutional codes presented in this section is adopted from [25]. The bounds are used later to estimate the goodput of the SCW and MCWs adaptive systems.

The packet error rate of rate *k/n* convolutional code is defined as the probability of deciding an incorrect codeword. It is bounded by [25]:

$$PER < \sum_{d=d_{free}}^{\infty} X_d P_d \qquad (4.1)$$

where X_d is the number of incorrect paths of a distance d that diverge then remerge with the correct path; P_d is the probability deciding an incorrect path which is the pairwise error probability, and d_{free} is the minimum distance of the code.

If the total number of information bits in the codeword is B then there are B/k branches along the correct path in the trellis. Each node has A_d error events of weight d that diverge from it and remerge at the correct path later. Thus, X_d can be bounded by [8]:

$$X_d \le \frac{B}{k} A_d \qquad (4.2)$$

The inequality in (4.2) is because the finite codeword length may not include all the $\frac{B}{k}A_d$ codewords. Assuming L coded bits in the codeword the upper bound for the PER takes the form:

$$PER \leq \frac{B}{k}\sum_{d=d_{free}}^{L} A_d P_d \qquad (4.3)$$

The bound to bit error probability of the convolutional code is given by [21]:

$$BER \leq \frac{1}{k}\sum_{d=d_{free}}^{L} C_d P_d \qquad (4.4)$$

where C_d is the total number of information bit errors produced by the all incorrect paths of weight d.

$A_{d,}$ C_d and d_{free} depend on the code structure and they are obtained by a computer search of the trellis over all the possible codewords [21] [25], while P_d depends on the channel and the modulation used for transmission, and is independent of the code itself. The rate half convolutional encoder used in this work has a generator polynomial (171, 133). Higher rates are obtained by puncturing the rate ½ mother codeword. The distance spectrum of the different rates used in this work, and their associated puncturing patterns are listed in Table 4.1; they are obtained using a computer search, some of them are also present in [26]. Note that, the listed distance properties are for terminated codes, unterminated codes have different distance spectrum.

Table 4.1: Distance spectrum of the terminated punctured convolutional code

Rate *(k/n)*	Puncturing pattern	d_{free}	A_d at $d=\{d_{free}, d_{free}+1, d_{free}+2, \ldots d_{free}+7\}$ C_d at $d=\{d_{free}, d_{free}+1, d_{free}+2, \ldots d_{free}+7\}$
½	1 1 1 1	10	A_d=[11, 0, 38, 0, 143, 0, 1331, 0] C_d =[36, 0 211, 0, 1404, 0, 11633, 0]
2/3	1 0 1 1	6	A_d=[1, 16, 48, 158, 642, 2435, 9174, 34701] C_d =[3, 70, 285, 1276, 6160, 27128, 117019, 498835]
¾	1 0 1 1 1 0	5	A_d=]8, 31, 160, 892, 4512, 23297, 120976, 624304] C_d =[42, 201, 1492, 10469, 62935, 379546, 2252394, 13064540]

In the following analysis the pairwise error probability (P_d) is obtained assuming BPSK modulation and AWGN environment. The received signal can be expressed as:

$$y_i = x_i + u_i \qquad (4.5)$$

where u_i is the Gaussian noise affecting symbol i in the codeword, x_i is the i^{th} transmitted symbol, where $i=\{1, 2, \ldots, W\}$, and W is the total number of transmitted symbols in the codeword.

The probability of the received signal given the transmitted symbol ($P(y_i / x_i)$) has a Gaussian distribution with mean x_i and variance $\frac{N_o}{2}$. It is given by:

$$P(y_i / x_i) = \sqrt{\frac{1}{\pi N_o}} \exp(-\frac{(y_i - x_i)^2}{N_o}) \qquad (4.6)$$

Assuming a memoryless channel, which is a valid assumption using perfect interleavers, the metric of viterbi decoding (the log-likelihood function) is expressed as follows:

$$M(y/x) = \ln p(y/x) = \ln \prod_{i=0}^{W-1} P(y_i/x_i) = \sum_{i=0}^{W-1} \ln P(y_i/x_i) \qquad (4.7)$$

$$\sum_{i=0}^{W-1} \ln P(y_i/x_i) = -\frac{W}{2}\ln(\pi N_o) - \frac{1}{N_o}\sum_{i=0}^{W-1}(y_i - x_i)^2 \qquad (4.8)$$

$$\sum_{i=0}^{W-1} \ln P(y_i/x_i) = -\frac{W}{2}\ln(\pi N_o) - \frac{1}{N_o}\sum_{i=0}^{W-1}(y_i^2 - 2y_i x_i + x_i^2) = C_1 + C_2\sum_{i=0}^{W-1} y_i x_i \qquad (4.9)$$

where C_1 and C_2 are constants for all codewords. Since C_2 is a positive constant then it is required to choose the trellis path that maximizes the correlation between the received signal and the transmitted codeword ($y.x$).

The pairwise error probability (P_d) is to choose the codeword x' instead of the codeword x. Assuming soft demodulation, P_d can be expressed as:

$$P_d = \Pr(M(y/x') > M(y/x)) = \Pr\left(\sum_{i=0}^{W-1} r_i x_i' > \sum_{i=0}^{W-1} y_i x_i\right) \qquad (4.11)$$

Assuming the transmitted codeword is the all zeros codeword, such that: $x = (-\sqrt{Es}, -\sqrt{Es}.....,-\sqrt{Es})$. Without loss of generality we assume that the wrong codeword is different from the correct one in the positions from *i=1 to d.* Thus, we get:

$$P_d = \Pr\left(\sum_{i=1}^{d} y_i(\sqrt{Es}) - \sum_{i=1}^{d} y_i(-\sqrt{Es}) > 0\right) = \Pr\left(\sum_{i=1}^{d} y_i > 0\right) \quad (4.12)$$

The term $\sum_{i=1}^{d} y_i$ is the sum of d independent random variables each has a mean of $-\sqrt{Es}$ and a variance of $\frac{N_o}{2}$. Let $\rho = \sum_{i=1}^{d} y_i$ Then,

$$\Pr(\rho > 0) = \sqrt{\frac{1}{\pi dNo}} \int_0^{\infty} \exp\left(\frac{-(\rho + d\sqrt{Es})^2}{dNo}\right) d\rho \quad (4.13)$$

Let $s = \left(\rho + d\sqrt{Es}\right)\sqrt{\frac{2}{dNo}}$ then,

$$\Pr(\rho > 0) = \sqrt{\frac{1}{2\pi}} \int_{d\sqrt{\frac{2Es}{dNo}}}^{\infty} \exp\left(\frac{-s^2}{2}\right) ds = Q\left(\sqrt{\frac{2dEs}{No}}\right) \quad (4.14)$$

Thus using BPSK the pairwise error probability is given by:

$$P_{d,BPSK} = Q\left(\sqrt{\frac{2dE_s}{No}}\right) \quad (4.15)$$

Substituting in (4.3) and (4.4) we get the PER and BER bounds as follows:

$$PER \le \frac{B}{k} \sum_{d=d_{free}}^{L} Ap_d Q\left(\sqrt{\frac{2dE_s}{No}}\right) \quad (4.16)$$

$$BER \le \sum_{d=d_{free}}^{L} C_d Q\left(\sqrt{\frac{2dE_s}{No}}\right) \quad (4.17)$$

Using QPSK modulation the pairwise error probability is given by [12]:

$$P_{d,QPSK} = Q\left(\sqrt{\frac{dE_s}{No}}\right) \qquad (4.18)$$

While for the 16-QAM the pairwise error probability is given by [12] [27]:

$$P_{d,16QAM} \approx \frac{1}{I_d}\sum_{k=0}^{\lfloor d/3 \rfloor}\sum_{m=0}^{\left\lfloor \frac{d-3k}{4} \right\rfloor}\binom{\lfloor d/3 \rfloor}{k}\binom{\left\lfloor \frac{d-3k}{4} \right\rfloor}{m} Q\left(\sqrt{\frac{d+2k+4m}{5}\frac{E_s}{N_o}}\right) \qquad (4.19)$$

where:

$$I_d = \sum_{k=0}^{\lfloor d/3 \rfloor}\sum_{m=0}^{\left\lfloor \frac{d-3k}{4} \right\rfloor}\binom{\lfloor d/3 \rfloor}{k}\binom{\left\lfloor \frac{d-3k}{4} \right\rfloor}{m} \qquad (4.20)$$

The bounds for the convolutional code when QPSK and 16QAM are employed can be obtained by substituting in equations (4.3) and (4.4). The first term in the summation (at d_{free}) dominates the bound at high SNR values, and can be used to approximate the bound.

The approximation for the Q function used in the simulations is given by [28]:

$$Q(x) = \frac{1}{x(1-1/\pi)+(1/\pi)\sqrt{x^2+2\pi}}\frac{1}{\sqrt{2\pi}}\exp\left(-\frac{x^2}{2}\right) \qquad (4.21)$$

In Figure 4.1a the BER performance for the different rate combinations in AWGN environment is shown, where the simulation results and the upper bounds are plotted. Also, in Figure 4.1b the PER is simulated and upper bounded for the

different rates. In these figures the number of output symbols is confined to 108 symbols (this determines the number of information bits per codeword (B)).

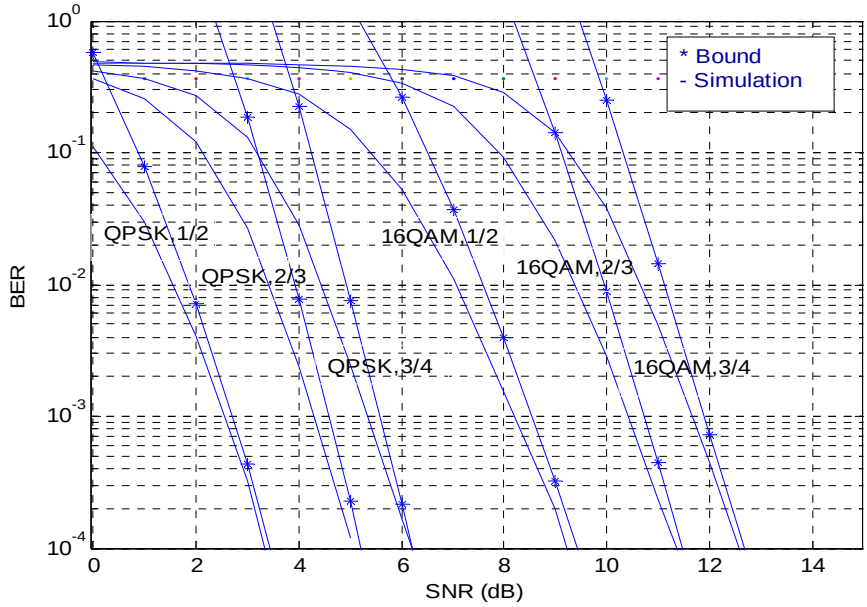

(a)

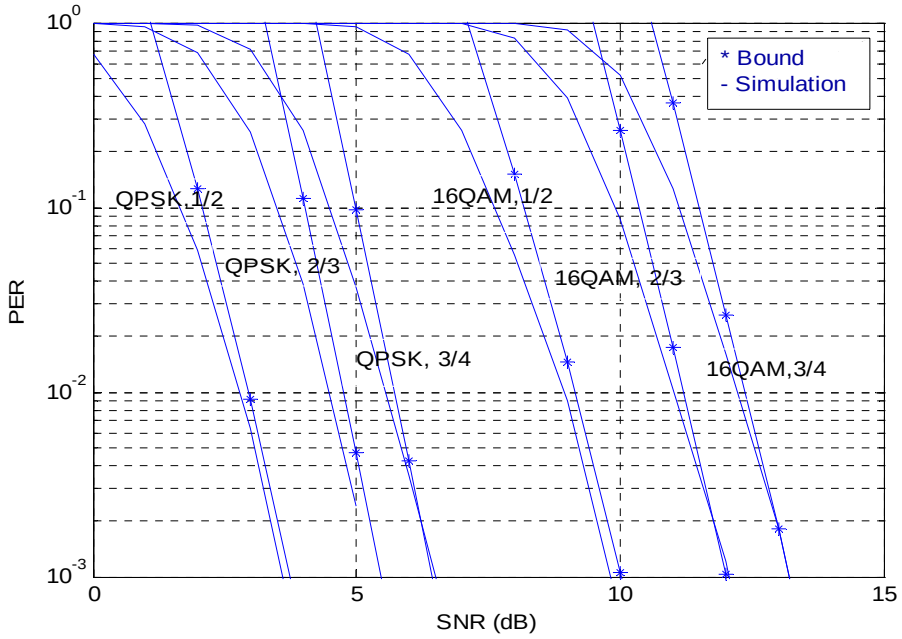

(b)

Figure 4.1: (a) Simulation and bound for BER, (b) Simulation and bound for PER for the different rate combinations in AWGN environment.

4.3 Fading channel model

The channel model used in the simulations is the ITU modified pedestrian B channel model where the velocity is 3km/hr [13]. Temporal correlation is maintained using Doppler spectrum. Table 4.2, shows the channel power and delay profile.

Table 4.2: Modified Pedestrian B profile

Path Index	Power (dB)	Delay (ns)
1	-1.175	0
2	0	40
3	-0.1729	70
4	-0.2133	120
5	-0.2661	210
6	-0.3963	250
7	-4.32	290
8	-1.1608	350
9	-10.4232	780
10	-5.7198	830
11	-3.4798	880
12	-4.1745	920
13	-10.1101	1200
14	-5.646	1250
15	-10.0817	1310
16	-9.4109	1350
17	-13.9434	2290
18	-9.1845	2350
19	-5.5766	2380
20	-7.6455	2400
21	-38.1923	3700
22	-22.3097	3730
23	-26.0472	3760
24	-21.6155	2870

The signal parameters can be found in [13], and are listed below:

- Carrier frequency: 10MHz.
- Sampling frequency: 11.2MHz.
- Bandwidth: 10MHz.
- FFT size: 1024.

4.4 Simulation results using Convolutional codes

4.4.1 Assumptions

- Rate 1/2 convolutional encoder in WiMAX IEEE802.16e with the generator polynomial (171,133) is used [23]. The same puncturing patterns as in the 802.16e standard are also employed, and are listed in Table 4.1.

- The tile is 18 subcarriers by six OFDM symbols. This is the tile size proposed by the IEEE 802.16 group handling the new WiMAX standard specifications (802.16m) in the IEEE 802.16m system description document [29]. We assume 18 tiles and, hence, 324 active subcarriers per OFDM symbol.

- The channel remains unchanged over six consecutive OFDM symbols and changes in the next frame where a frame is 5ms.

4.4.2 Constant Bit rate adaptive radio

We first investigate the performance of the proposed structure for SCW against the MCWs when it is required to transmit at a constant bit rate (CBR). For

CBR a single modulation scheme is allowed. We use QPSK since this might be required for some low end mobile devices where a low cost power amplifier precludes the use of 16QAM. Using a simple adaptive scheme, only three rates are assumed assumed (QPSK, 1/2) (QPSK, 2/3) and (QPSK, 3/4). The tiles are divided into three groups according to their average SNR and the three rates are assigned evenly over the tiles, such that a higher code rate is assigned to the group of the tiles that have larger average SNR and a lower rate is assigned to the group with lower average SNR. In Figure 4.2 and Figure 4.3, IntP, PDI, SCW with per tile interleaving (PTI), and MCWs are compared in terms of goodput and BER, respectively. The goodput (η) is defined as [24]:

$$\eta = \frac{1}{C}\sum_{i=1}^{C}(1 - PER_i) * B_i \qquad (4.22)$$

where C is the number of channel realizations, PER_i and B_i are the packet error rate and the number of bits per packet for channel i respectively. It is noted that for constant bit rate adaptive schemes B_i is fixed for all channel realizations, and here it is set to 2484 (bits/frame). The packet is received in error if any bit in the packet is not decoded correctly.

In the SCW structure, codes are terminated by appending six zeros at the end of the data sequence, while the MCWs structure requires six zeros to be appended at each tile for termination, which is a relatively large overhead and might be impractical for small tile sizes. In the simulation we compare the SCW against the terminated and the unterminated MCWs.

It is shown in Figure 4.2 that SCW with PTI has around 1dB gain over the unterminated MCWs at a goodput of 1500 bits. IntP outperforms the MCWs by 5dB. It is also shown that IntP provides 1dB gain over the PDI structure.

Optimizing the interleaver of the IntP might lead to even better results. If the MCWs are terminated, its performance is improved by around 1dB compared to the unterminated MCWs, hence achieving the same performance of the SCW with PTI at a goodput of 1500 bits. However at a higher SNR values the SCW with PTI saturates at a higher goodput value compared to the terminated MCWs, this is mainly due to the termination overhead required to terminate multiple encoders in the MCW structure.

Note that in CBR applications one cannot guarantee that a certain target BER is achieved regardless of the channel quality, since fixed rate data has to be transmitted in any case.

The BER curves for the different structures under CBR constraint are shown in Figure 4.3. It is clear that the IntP has around 1dB gain over the PDI structure at BER value of 10^{-2}. The teminated MCWs achieves almost the same error performance of the SCW with PTI, but with more termination overhead that is a function of the number of tiles. PDI still offers 4dB gain over the terminated MCWs.

It is noted from Figures 4.2 and 4.3 that the larger interleaver depth mainly contributes to the gain of the PDI and IntP structures over the MCWs. The SCW with PTI is almost achieving the same error performance as the terminated MCWs, with lower termination overhead. More gains are expected over the MCWs at a smaller tile sizes as will be illustrated in section 4.4.3.2.2.

The proposed IntP structure requires further investigations regarding its joint interleaved puncturing pattern. We leave this to be an area of future research. The rest of the simulations are concerned with the PDI structure for interleaving the SCW.

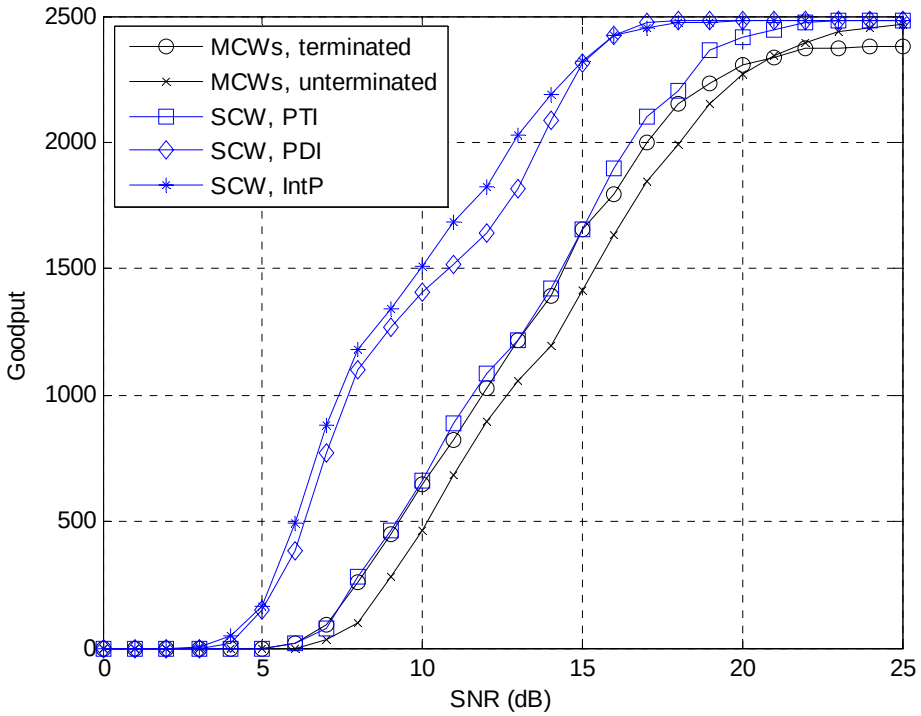

Figure 4.2: Goodput using CBR for convolutional code

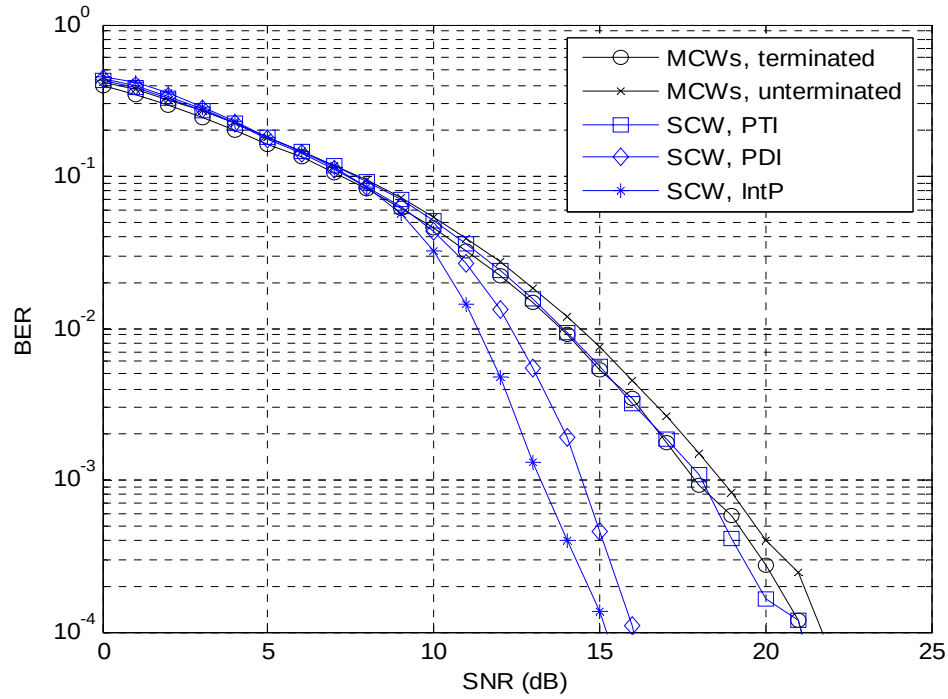

Figure 4.3: BER using CBR for convolutional code

4.4.3 Variable Bit rate adaptive radio

For variable bit rate applications, the recursive and MIESM schemes are used to determine the transmission parameters over the tiles. We use the PDI structure for interleaving the SCW and compare it against the MCWs and PFA. The different rate combinations used and their corresponding switching thresholds, under BER_{target} value of 10^{-2}, are listed in Table 4.3. The thresholds used for the MCWs are determined according to the codeword length that is limited to the tile size used later in the simulations which is 18 carriers by six OFDM symbols. However, PDI and PFA use codeword lengths equals to the frame size. The BER_{target} value of 10^{-2} achieves the highest goodput as will be illustrated later in the simulations.

Table 4.3: Different rate combinations used for convolutional code.

Index α	**Rate combination (modulation, code rate)**	**Thresholds (dB)** **($BER_{target}=10^{-2}$)**
0	No transmission	< 2.5
1	(QPSK, ½)	2.5
2	(QPSK, 2/3)	4
3	(QPSK, ¾)	5
4	(16QAM, ½)	8
5	(16QAM, 2/3)	10
6	(16QAM, ¾)	11.5

4.4.3.1 Recursive scheme

In this section we present the results of adaptively loading the tiles using the recursive scheme. In Figure 4.4, the recursive scheme is applied for PDI, MCWs and PFA with a maximum guaranteed error performance *(BER_{target})* of 10^{-2}. It is shown that at a goodput of 3000 bits the SCW with the PDI scheme outperforms the unterminated MCWs by 5dB and outperforms the PFA by around 13dB. The PDI also outperforms, in terms of goodput, the unterminated MCWs by 60% and the PFA by seven times at an SNR value of 15dB. The PDI has around 1dB gain over the terminated MCWs at a goodput value of 5000bits. The maximum goodput for zone loading (MCWs and PDI) is also plotted in the figure. The maximum goodput (throughput) is obtained from the adaptive scheme assuming zero packet errors and it can be expressed as:

$$\eta_{\max} = \frac{1}{C}\sum_{i=1}^{C} B_i \qquad (4.23)$$

It is shown that after 15dB the PDI is almost achieving the maximum goodput of the adaptive scheme.

Figure 4.5 shows the BER performance of the SCW and MCWs. It is noted that the target *BER* is not exceeded. It is also shown that the PDI has a strong error correcting capability and achieves the lowest error rates and is close to the MCWs error performance.

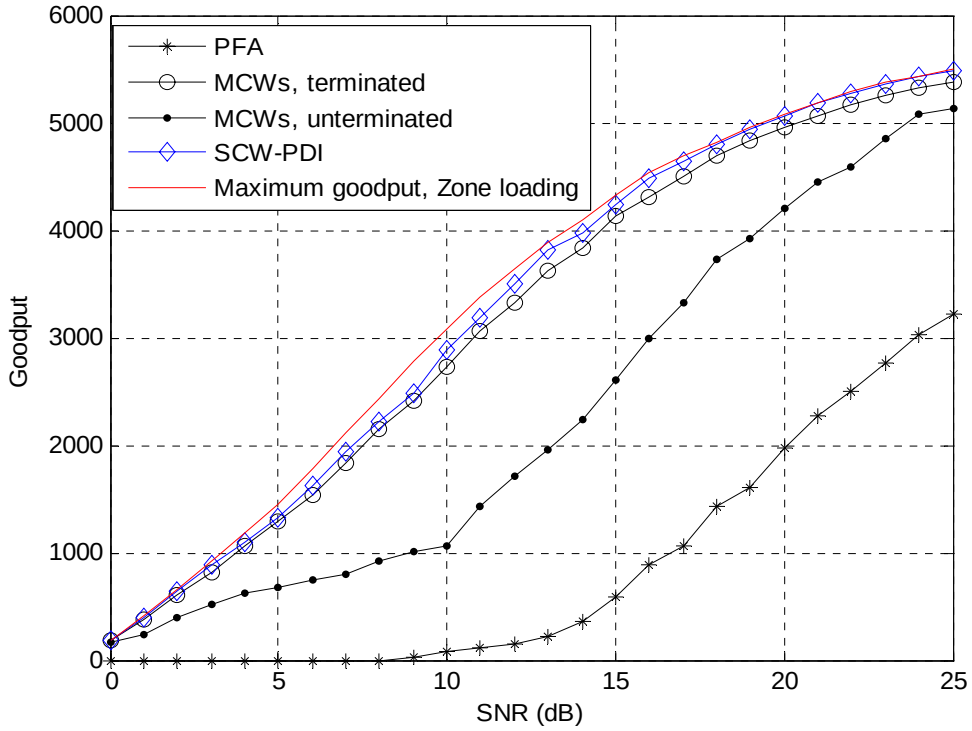

Figure 4.4: Goodput using recursive scheme

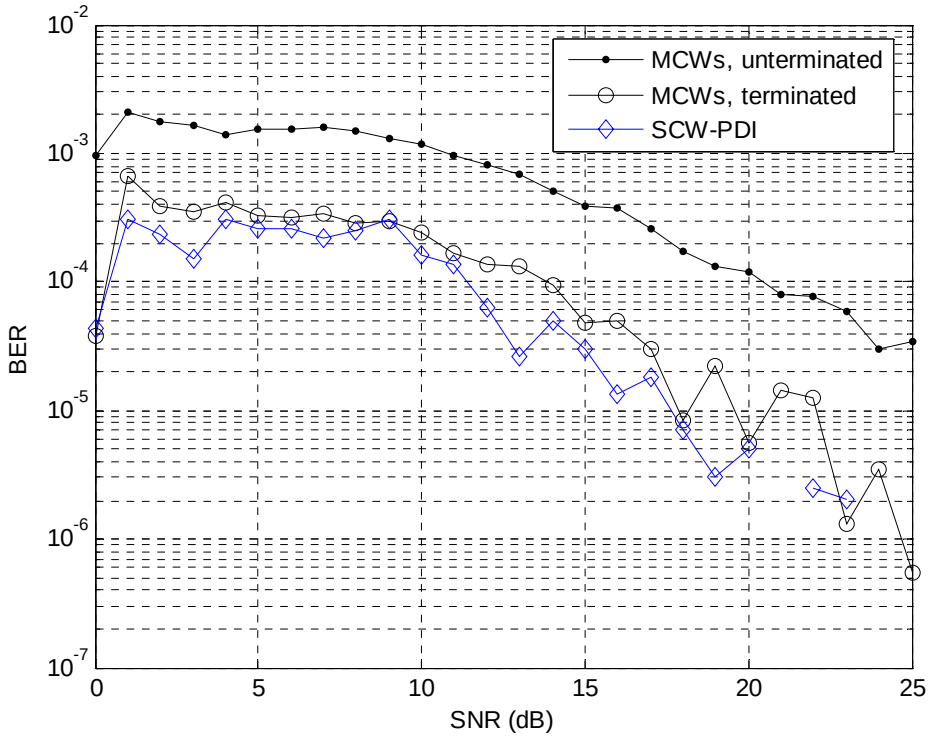

Figure 4.5: BER performance of SCW and MCWs using recursive scheme.

4.4.3.2 MIESM scheme

In this section the MIESM scheme is used for rate selection. It is shown in Figure 4.6 that the PDI has a gain of 8dB over the unterminated MCWs and a gain of around 3dB over the PFA at the same goodput value of 2000 bits. The PDI achieves almost the same performance as the terminated MCWs.

The error performance of the MCWs and SCW is shown in Figure 4.7. It is noted that the terminated MCWs and the PDI have the same error performance, which is much improved than the unterminated MCWs.

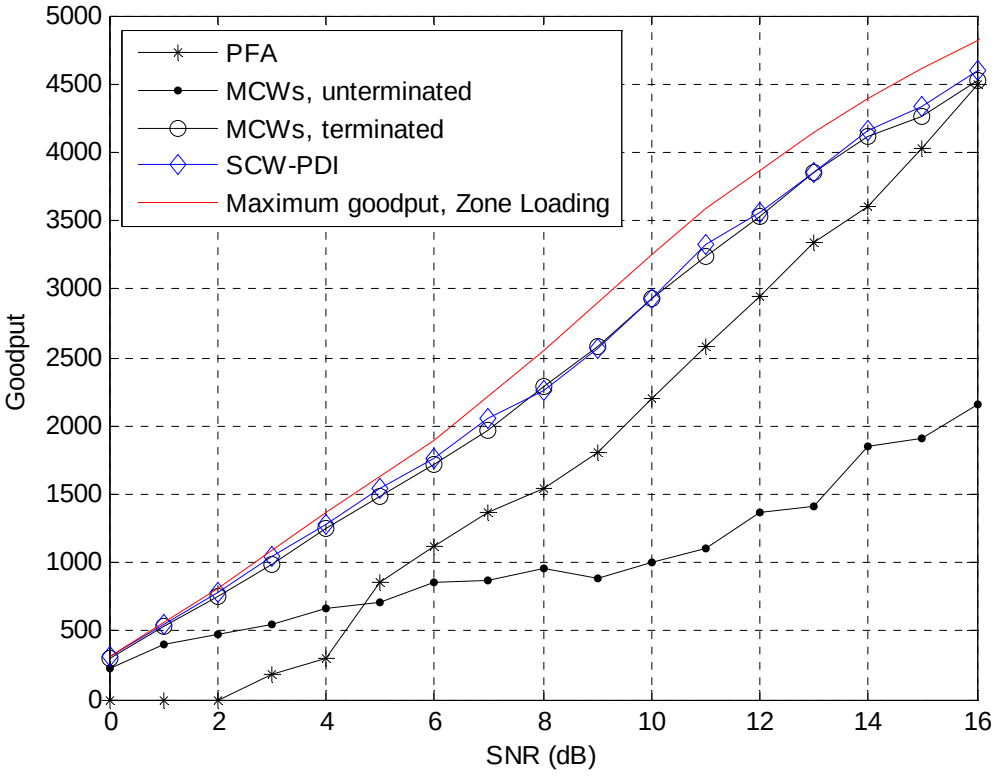

Figure 4.6: Goodput using MIESM scheme

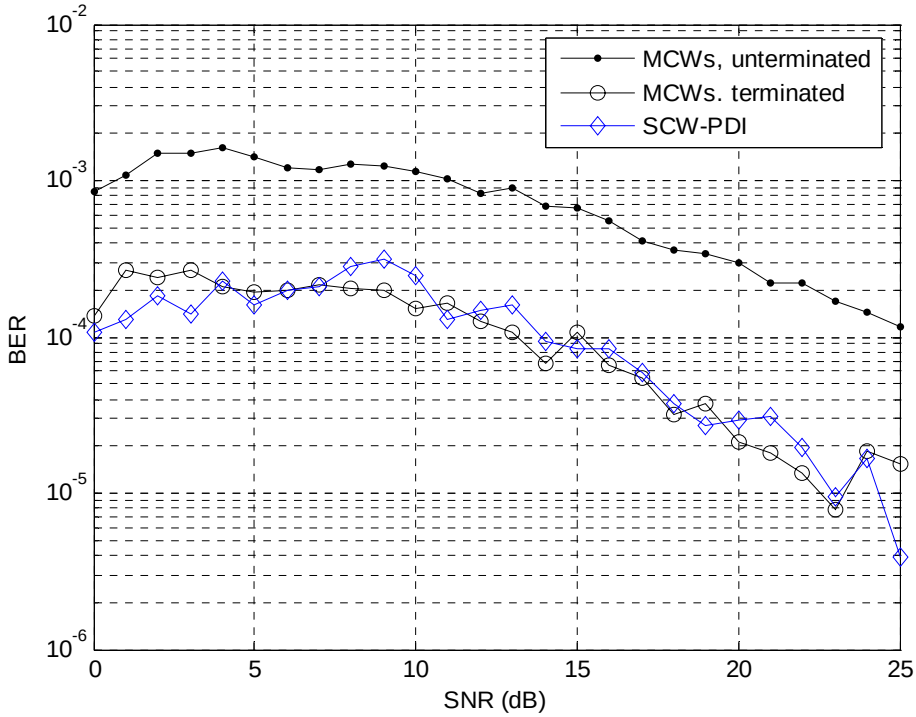

Figure 4.7: BER performance of PFA, PDI and MCWs using the MIESM scheme

From Figures 4.4 and 4.6, it is noticed that the PFA is improved significantly using the MIESM scheme if compared to the recursive method. Using MIESM, PFA is improved by around 78% in goodput compared to using the recursive scheme at 18dB SNR value. This is because the effective SNR obtained from MIESM mapping is a better representative for the channel quality than the average BER used in the recursive scheme. As the linear average of the BER is dominated by the severely attenuated carriers that has very high BER values.

The MIESM scheme is compared against the recursive method, for the SCW and the terminated MCWs in Figure 4.8. It is shown that the MIESM scheme is superior to the recursive rate selection method for both MCWs and SCW. It is also noted that PDI is outperforming the terminated MCWs using either the MIESM or the recursive scheme. In the rest of the simulations we investigate

the performance of the proposed adaptive puncturing system using the MIESM based schemes.

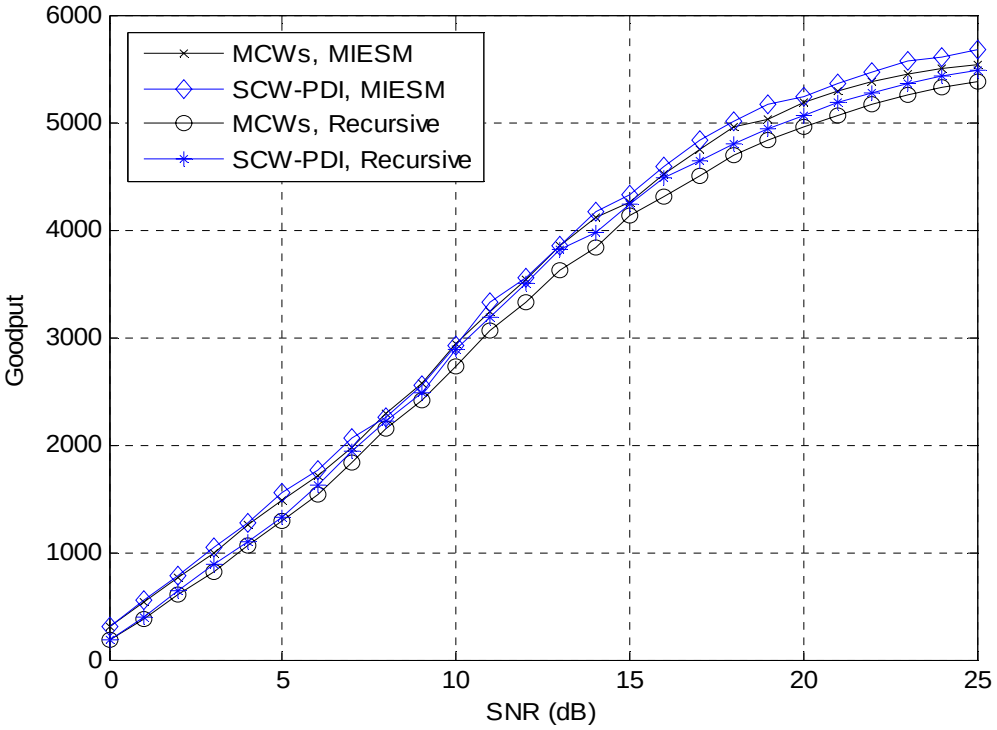

Figure 4.8: Recursive Vs the MIESM schemes for SCW-PDI and MCWs.

The effect of targeting different bit error rates is shown in Figure 4.9. The goodput of the SCW-PDI structure under MIESM rate selection scheme is plotted. It can be shown that a target BER of 10^{-2} achieves the highest goodput compared to a target BER of 10^{-1}, 10^{-3} or 10^{-4}.

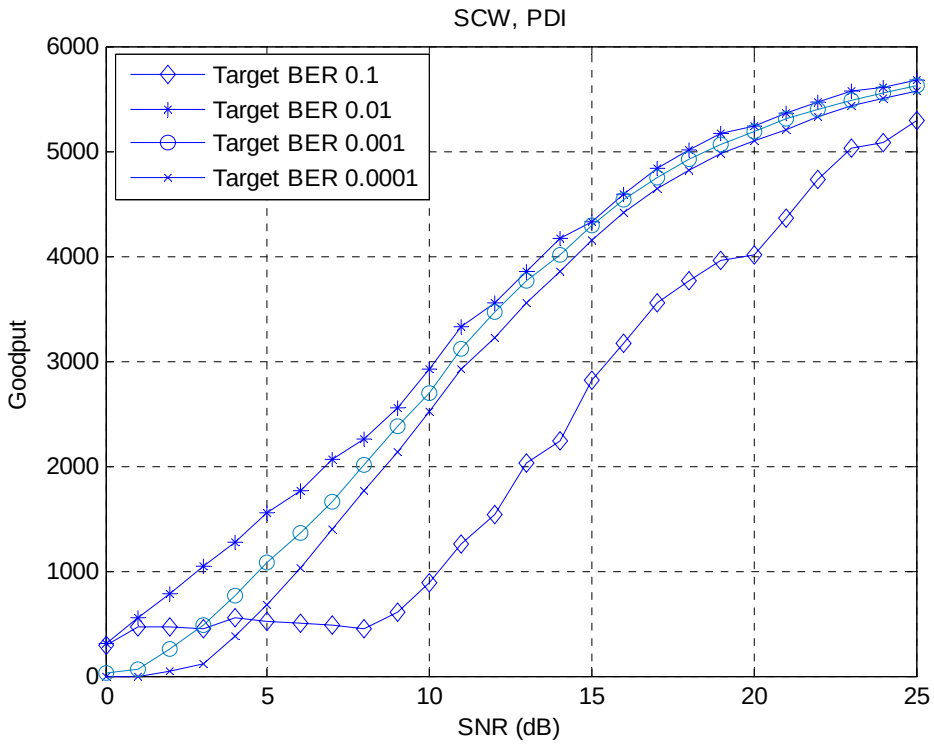

Figure 4.9: Goodput of PDI structure at different target bit error rates

4.4.3.2.1 Goodput estimation

In order to check the correctness of our simulations, we estimate the goodput for the SCW and the MCWs structures under MIESM scheme. First we illustrate via simulation the distribution of the information bit error rate along the frame in case of the non-uniform punctured SCW and the terminated MCWs. In this simulation, shown in Figure 4.10, two tiles are used for transmission. The first tile has SNR value of 2.5dB such that it transmits with (QPSK, 1/2), while the second has SNR value of 5dB such that it transmits with (QPSK, 3/4). Thus, the first tile holds 102 information bits, in the MCWs case, and the second holds 156 information bits. However, for the SCW the first tile hold 108 information bits. It can be shown that the error distribution is almost the same for the SCW and the MCWs, except at the transition region between the two tiles where the MCWs structure has lower error rates due to termination.

In our analysis for goodput estimation we assume that each tile can be considered as a separate packet. The tile packet error rate can be bounded by equation (4.3), and by ignoring the transitions in the SCW, the distance spectrum used for each tile is that of the terminated codes.

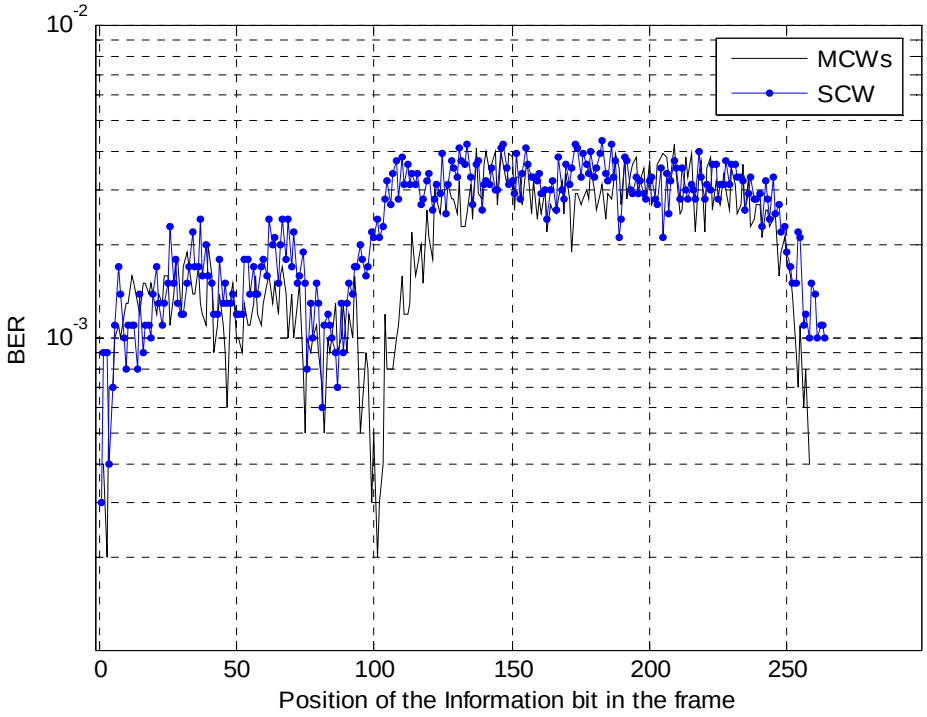

Figure 4.10: BER at each information bit position.

Goodput estimation is obtained for the MCWs and the SCW by first estimating the PER for each channel realization i ($PER_{est,i}$) as follows:

For SCW:

$$PER_{est,i} = \sum_{t=1}^{T} TER_t \qquad (4.24)$$

For MCWs:

$$PER_{est,i} = 1 - \prod_{t=1}^{T} (1 - TER_t) \qquad (4.25)$$

Such that TER_t is the estimated tile error rate for tile t and T is the number of tiles.

The effective SNR (SNR_{eff}) value is obtained for each tile using MIESM mapping scheme and according to the assigned modulation order. By the obtained SNR_{eff}, AWGN expressions for pairwise error probability, in equations (4.18) and (4.19), can be directly used according to the assigned modulation. TER_t can be determined from equation (4.3) with the aid of Table 4.1. Only the term at d_{free} is used for evaluating TER_t in order to have an approximate value for the PER and hence the goodput. According to the estimated PER the goodput (GP_{est}) can be determined as follows:

$$GP_{est} = \frac{1}{C}\sum_{i=1}^{C}\left(\left(1 - PER_{est,i}\right)\times B_i\right) \qquad (4.26)$$

where B_i is the number of bits per frame for the i^{th} channel realization and it is obtained through measurements by applying the adaptive scheme, and C is the number of channel realizations.

The result of the estimation is shown in Figure 4.11. It is noted that the analytical estimate of the goodput for the SCW and the MCWs is within 1.5dB only from their simulated results, which also shows that the estimation approach followed is acceptable.

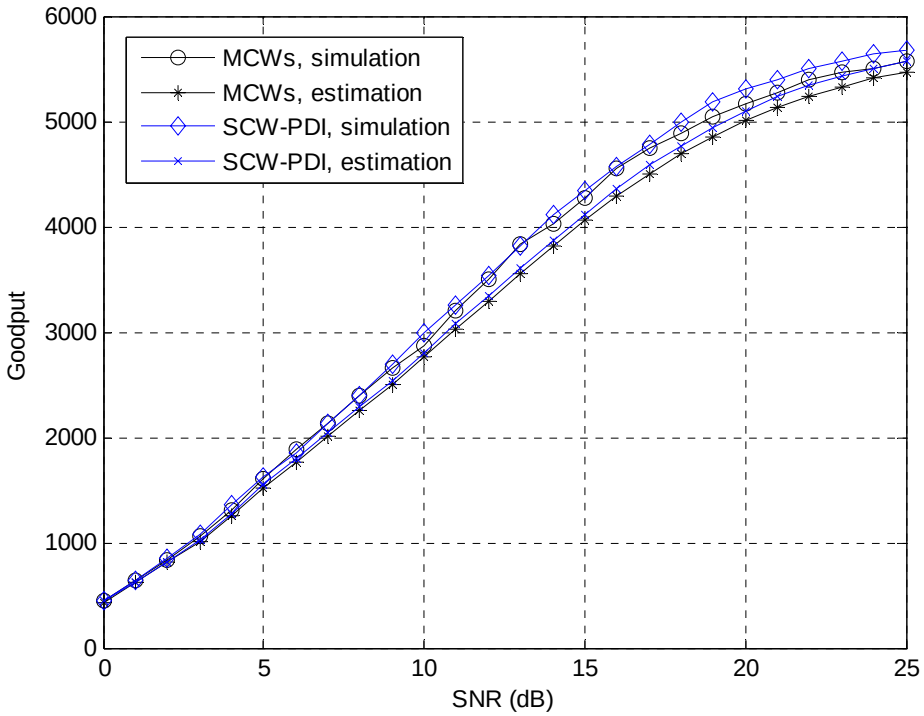

Figure 4.11: Goodput estimation of the terminated MCWs and SCW using MIESM adaptive scheme.

4.4.3.2.2 Tile size effect

From the simulations and analytical results presented so far, it can be seen that under variable rate adaptive schemes the terminated MCWs for the considered tile size, which is 18 subcarriers by six OFDM symbols, is almost achieving the same performance as the SCW. Terminating the MCWs is not practical if the tile size is very small as the termination overhead will reduce the overall goodput significantly. In Figure 4.12 the tile size is three subcarriers by six OFDM symbols and 108 tiles per frame are used maintaining 324 active subcarriers per OFDM symbol. It is shown from the figure that the PDI has around 5dB gain over the MCWs at a goodput of 4000bits.

It is noted that using the proposed SCW structure, small tile sizes can be employed without confining the codeword length and with much reduced termination overhead. In Figure 4.13 the normalized goodput per carrier, for the SCW and the MCWs, is plotted versus the tile size at SNR value equals to 10dB. The normalized goodput per carrier is obtained by dividing equation (4.22) by the total number of carriers per OFDM frame. In Figure 4.13 the number of carriers per OFDM symbol is fixed to 300, except for the 9*6 and 18*6 tile sizes where the number of carriers per OFDM symbol is fixed to 324 and for the 48*6 tile size where the number of carriers per OFDM symbols is fixed to 336. It can be shown that the SCW has considerable gains over the MCWs at small tile sizes. Such that at a tile size of three carriers by six OFDM symbols the SCW provides around 0.5 bits per carrier gain over the MCWs. This gain decreases as the tile size increases. It can be noticed that smaller tile sizes achieve better performance for the SCW, since they generally offer more degrees of adaptation.

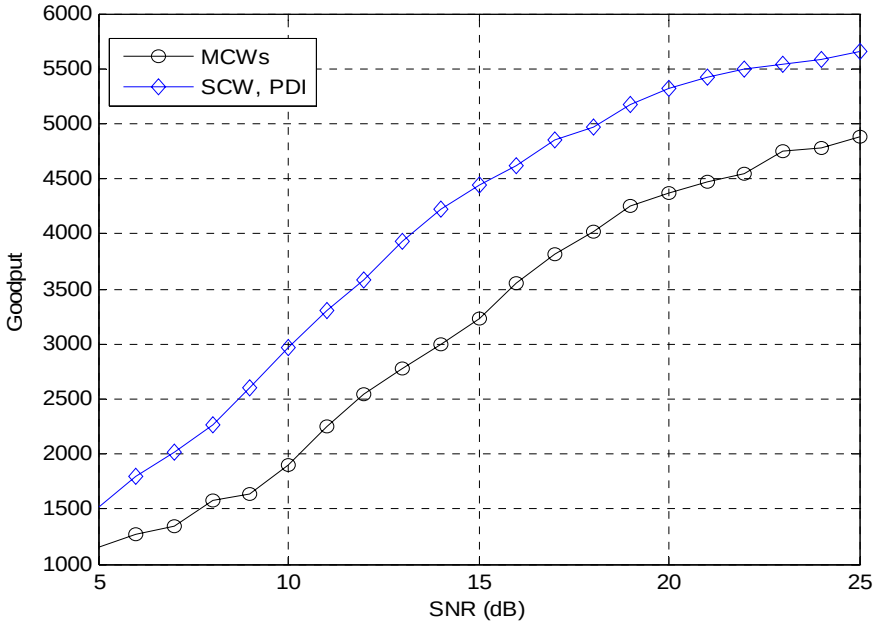

Figure 4.12: Goodput of PDI and MCWs when the tile size is 3*6.

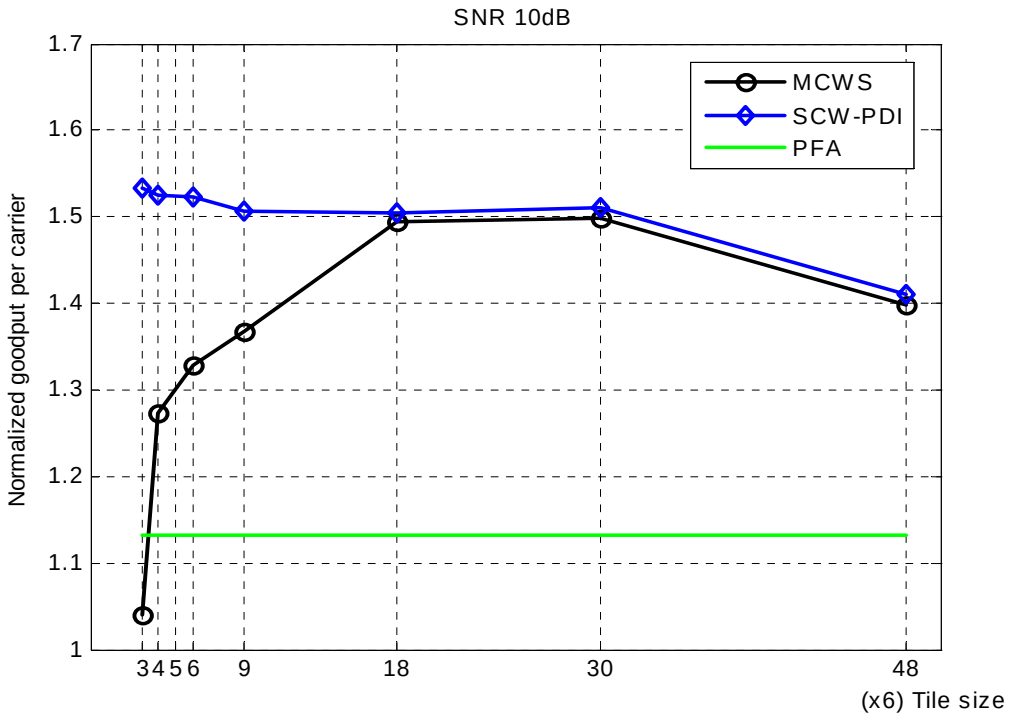

Figure 4.13: Normalized goodput per carrier, for SCW and MCWs, Vs the tile size.

4.5 Simulation Results using Turbo codes

The adaptive puncturing technique can be applied with turbo codes as illustrated in chapter 3. It is noted that for turbo codes no interleaver is employed between the coding and the modulation and only the turbo interleavers are used, as in the IEEE802.16e standard [23]. In this section we present the simulation results examining the SCW structure for turbo codes under CBR and variable bit rate adaptive schemes. The MIESM and R-MIESM are used to obtain variable bit rate adaptive system.

4.5.1 Assumptions

- The tile is 16 subcarriers by six OFDM symbols.

- The channel remains unchanged over six consecutive OFDM symbols and changes in the next frame where a frame is 5ms.

The BER performance of the different rate combinations used for turbo codes are shown in Figure 4.14, where the turbo block size is limited to the tile size used.

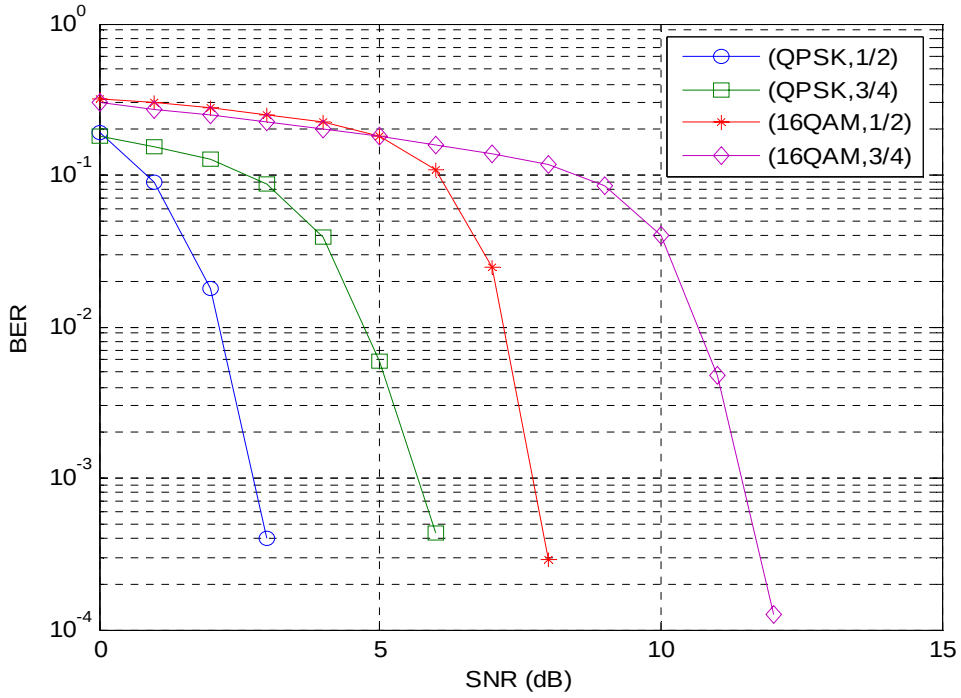

Figure 4.14: BER curves using Turbo codes

4.5.2 Constant bit rate adaptive radio

First the performance of the SCW is compared to the MCWs in a constant bit rate context, where a fixed information bits are transmitted in each frame. We assume a fixed data payload of 2400 (bits/frame). In this case we apply our fixed rate adaptive scheme discussed in the previous chapter, allowing only two rate combinations (QPSK, ½) and (QPSK, ¾) to be assigned evenly over tile, such that the best nine tiles use (QPSK, ¾) and the worst nine tiles use (QPSK, ½).

Employing four turbo iterations Figure 4.15 and Figure 4.16 show the goodput and BER performance of the different structures.

It is shown in Figure 4.15, that at a goodput of 2000 bits the SCW outperforms the MCWs by around 8dB, it is also shown in Figure 4.16 that at BER of 10^{-3} there is around 7dB gain from the SCW over the MCWs structure. This gain is because the SCW structure enables the use of larger block sizes and consequently larger turbo interleavers which significantly affects the decoder performance providing a strong error correcting capability.

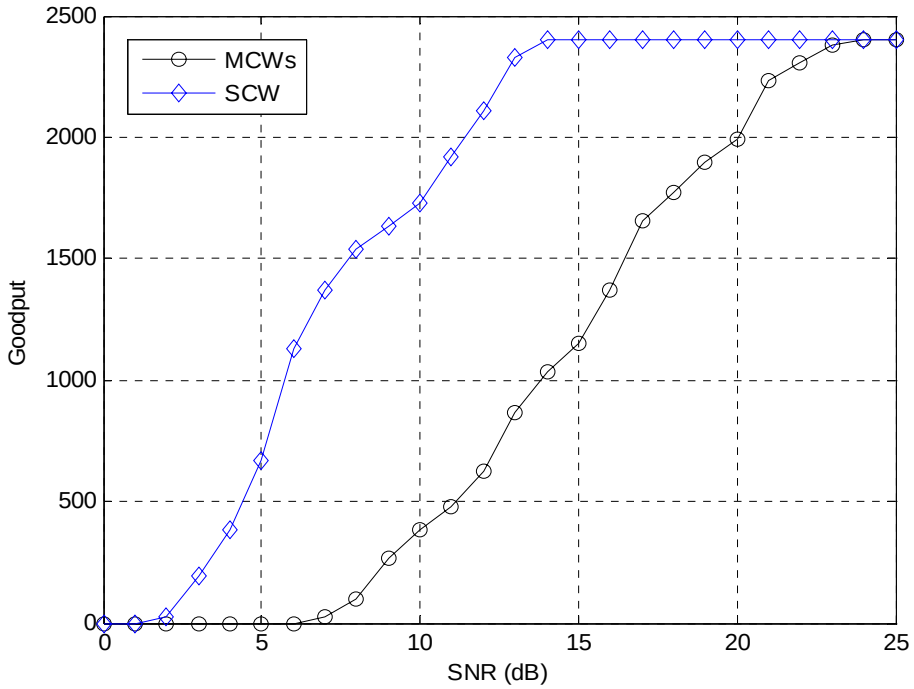

Figure 4.15: Goodput performance of SCW and MCWs under constant bit rate constraint using turbo codes, and four decoding iterations

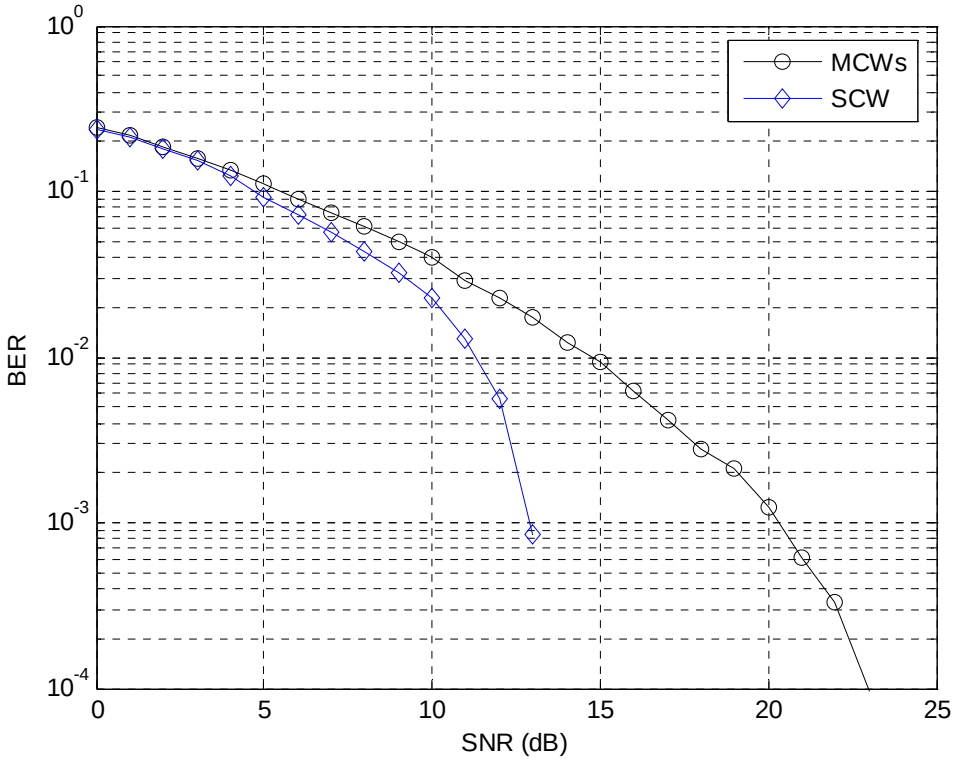

Figure 4.16: BER performance of SCW and MCWs under constant bit rate constraint using turbo codes, and four decoding iterations.

4.5.3 Variable bit rate adaptive radio

4.5.3.1 MIESM Scheme

In this section the performance of the SCW is investigated using MIESM based schemes (MIESM, and R-MIESM schemes). The different rate combinations used in the simulations are listed in Table 4.4.

Table 4.4: Different rate combinations used for turbo codes

Index α	**Rate combination (modulation, code rate)**
0	No transmission
1	(QPSK, ½)
3	(QPSK, ¾)
4	(16QAM, ½)
6	(16QAM, ¾)

Using two turbo decoding iterations, Figure 4.17 shows the performance of the SCW compared to the MCWS and the PFA. There is about 3dB gain of the proposed SCW structure over the MCWs, and around 2dB gain over the PFA at goodput value of 2500 bits.

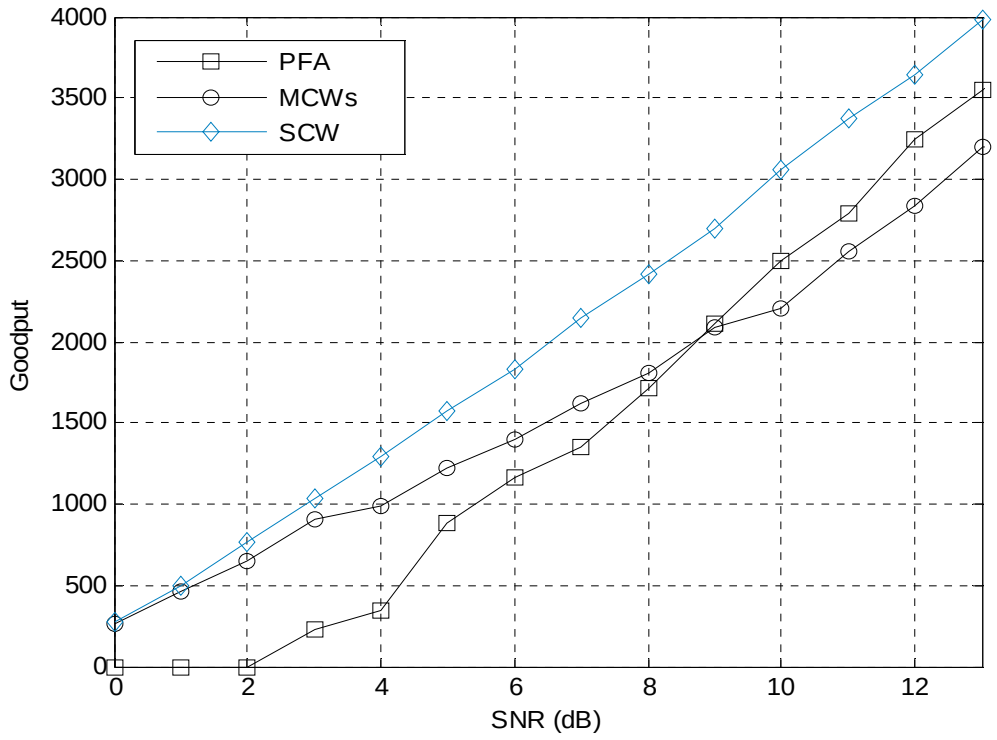

Figure 4.17: Goodput of SCW, MCWs and PFA using the MIESM scheme with two turbo decoding iterations.

In Figure 4.18 MIESM rate selection is employed and four turbo decoding iterations are used. The MCWs is improved by using four turbo iterations compared to using two iterations only; however the SCW still has around 1dB improvement in the performance over the MCWs. It is shown in the figure that the SCW is almost achieving the maximum goodput obtained from the MIESM adaptive scheme. It is also clear that the zone loading is superior to the PFA especially at low SNR values. At SNR values, higher than 8dB, the MCWs has around 0.7dB gain over the PFA although the PFA uses larger block size and hence larger interleavers, and the SCW provides around 2dB gain over PFA. It is noted that if higher rates are employed (ex. Add 64QAM), zone loading will show higher gains over the PFA.

The BER curves of the SCW and the MCWs using MIESM scheme are plotted in Figure 4.19. It is noticed that the SCW provides much improved error performance, such that its BER is about a decade lower than the BER level of MCWs structure. This indicates that the thresholds for the SCW could be adjusted such that higher rates could be selected, without exceeding the BER performance requirement.

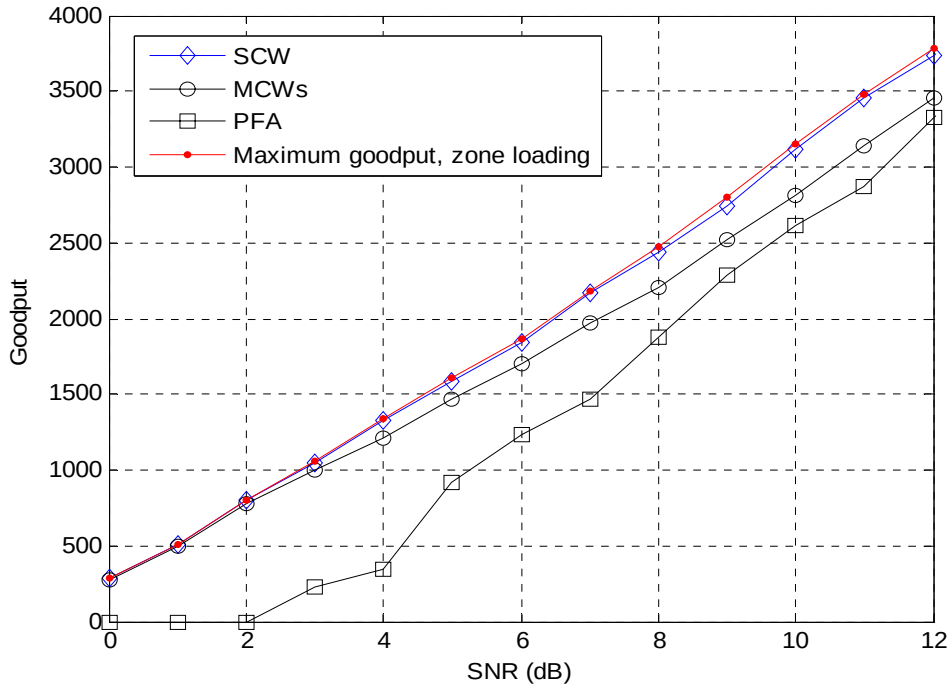

Figure 4.18: Goodput using the MIESM scheme, with four turbo decoding iterations.

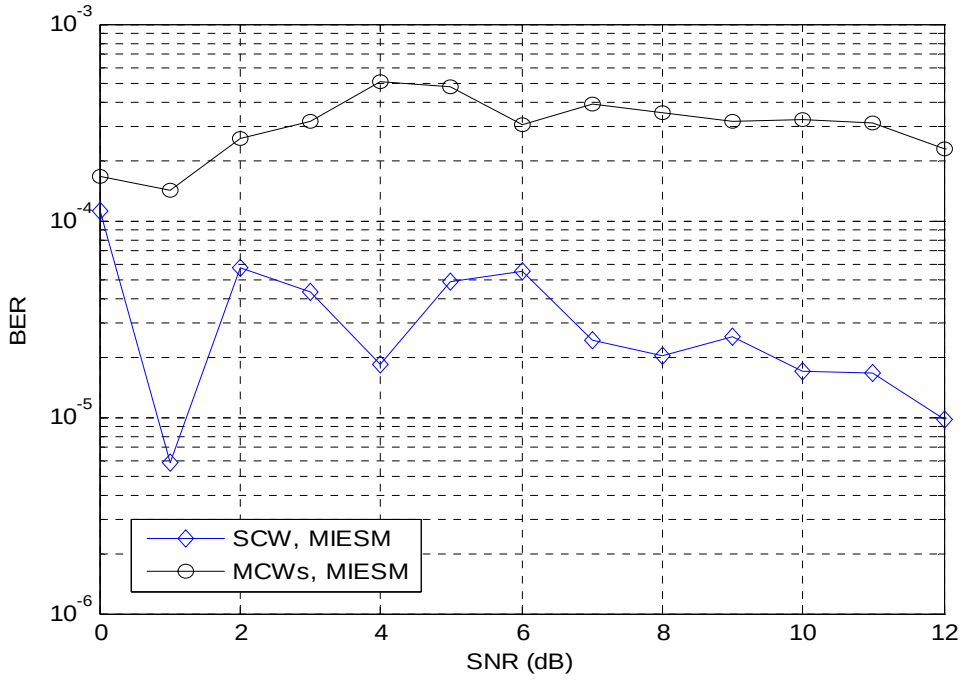

Figure 4.19: BER performance using the MIESM scheme with four turbo decoding iterations.

4.5.3.1.1 Tile size effect

We further extend the above results for turbo code by investigating the tile size effect. In Figure 4.20, the normalized goodput per carrier is plotted at SNR value of 10dB. There are 160 carriers per frame for the 8*6 tile size and the 16*6 tile size, 168 carriers per frame for the 24*6 tile size and 144 carriers per frame for the 48*6 tile size. For the SCW it is shown that small tile sizes provide improved goodput performance since higher degrees of adaptation are obtained. The SCW has 0.25 bits per carrier gain over the MCWs at a tile size of eight carriers by six OFDM symbols. The gain of the SCW over the MCWs decreases as the tile size increases, since larger tile sizes enables the MCWs to use larger turbo block sizes. The MCWs reaches a maximum normalized goodput of 1.6 bits per carrier at tile size of 24 carriers by six OFDM symbols. At a tile size of 48 carriers by six symbols the MCWs are expected to use even larger block sizes but due to dividing the frame into only three tiles the gain of tile adaptation is reduced, but still outperforming the PFA.

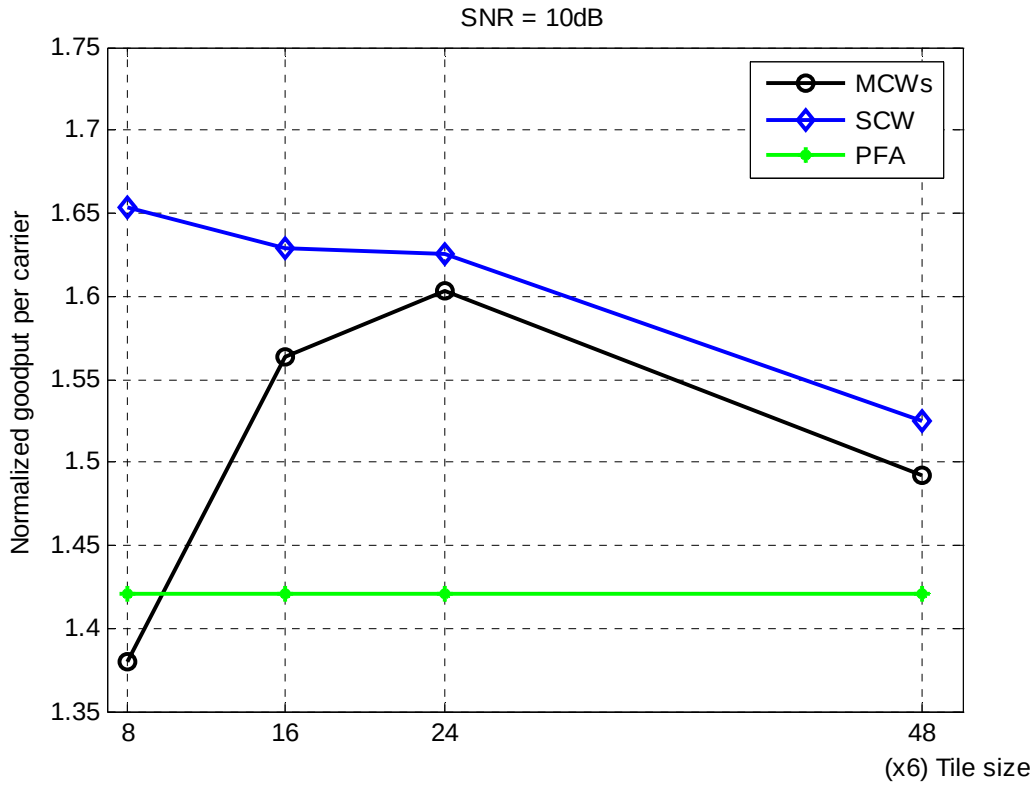

Figure 4.20: Normalized goodput per carrier performance obtained by applying MIESM scheme to turbo coded system.

4.5.3.2 R-MIESM Scheme

As discussed in the previous chapter, the R-MIESM scheme aims at choosing higher rate combinations over tiles, by exploiting the frequency diversity the SCW provides. In Figure 4.21 the R-MIESM is applied to the SCW and it is shown that it provides some improvement. The tile size is 16 subcarriers by six symbols. A gain of more than 1dB at a goodput of 5000 bits is obtained over the SCW with MIESM rate selection method. It can be noticed that the SCW with the R-MIESM can provide higher gains over the MCWs using MIESM scheme.

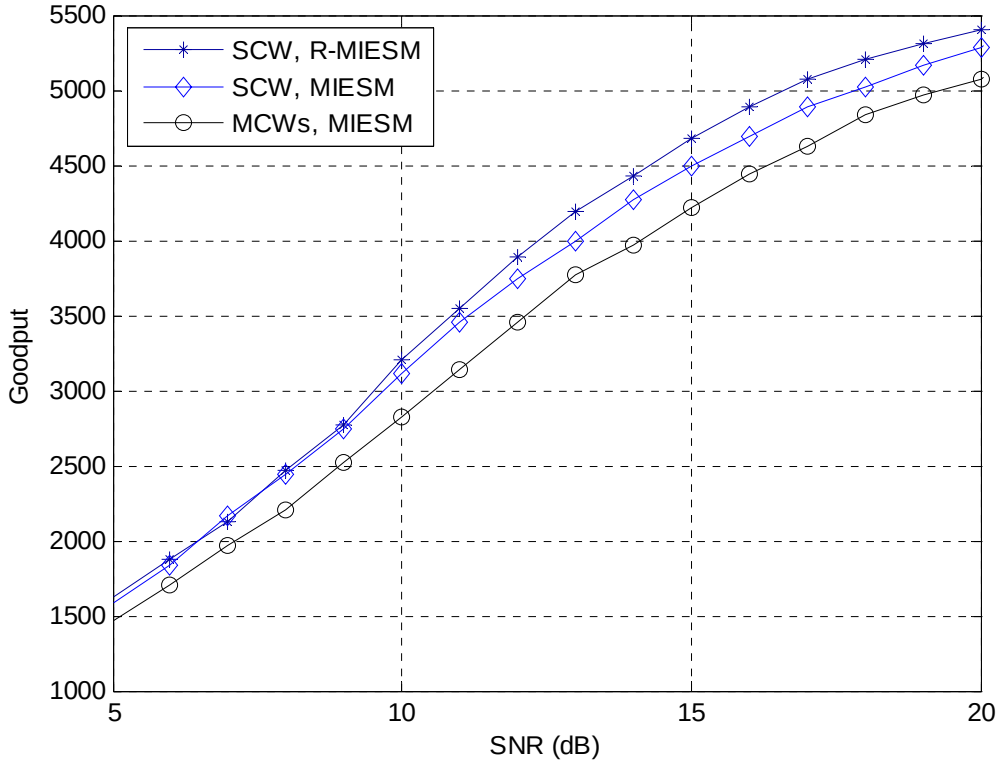

Figure 4.21: Goodput using the R-MIESM for SCW compared to using MIESM scheme, with four turbo decoding iterations.

The BER performance of the SCW employing R-MIESM and using four turbo iterations is shown in Figure 4.22. The SCW with R-MIESM scheme still achieves lower error rates than MCWs. The obtained BER for the SCW using the

R-MIESM scheme is higher than that obtained using MIESM scheme. That is mainly due to the higher rates that are selected when the R-MIESM scheme is employed for rate selection. It is noted that the SCW, using both rate selection methods, has a better error rate performance over the MCWs.

It can be noted from Figures 4.21 and 4.22 that using the R-MIESM scheme, higher error rates are present although the goodput is only improved at SNR values above 9dB. A better link quality metric, rather than the average BER of the frame, is needed. The link quality metric should be computed over the whole frame where non-uniform puncturing and different modulation schemes are considered. Investigating a better quality metric for the SCW is left for future study.

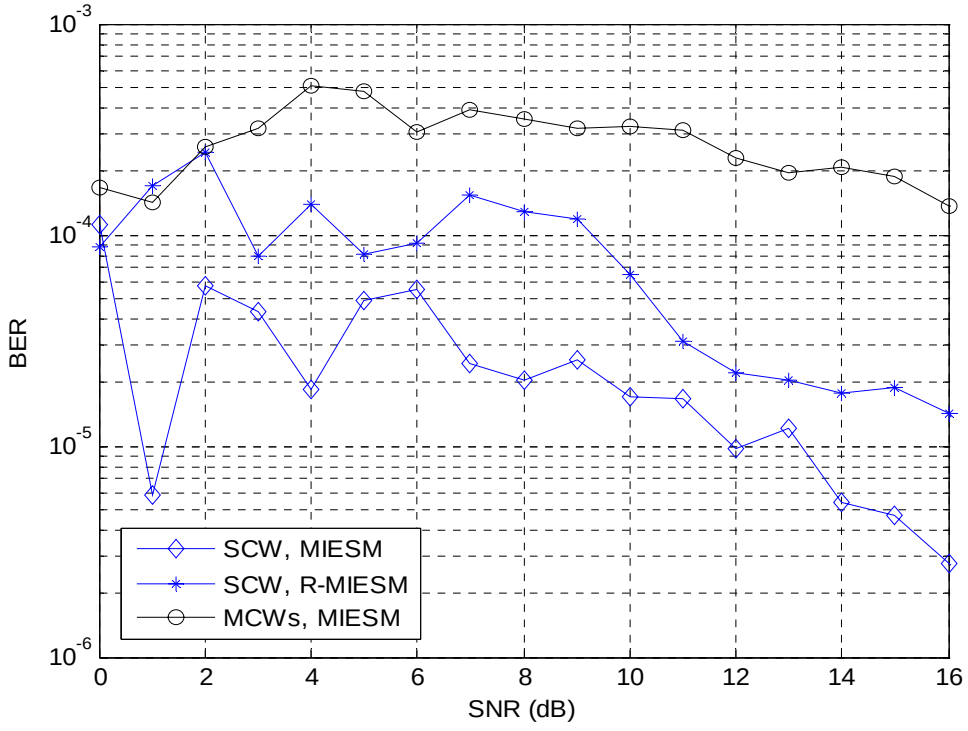

Figure 4.22: BER performance using the R-MIESM in the SCW compared to using MIESM, with four turbo decoding iterations.

The goodput of the R-MIESM compared to MIESM scheme using six turbo iterations is shown in Figure 4.23. No improvement is achieved compared to using four turbo iterations.

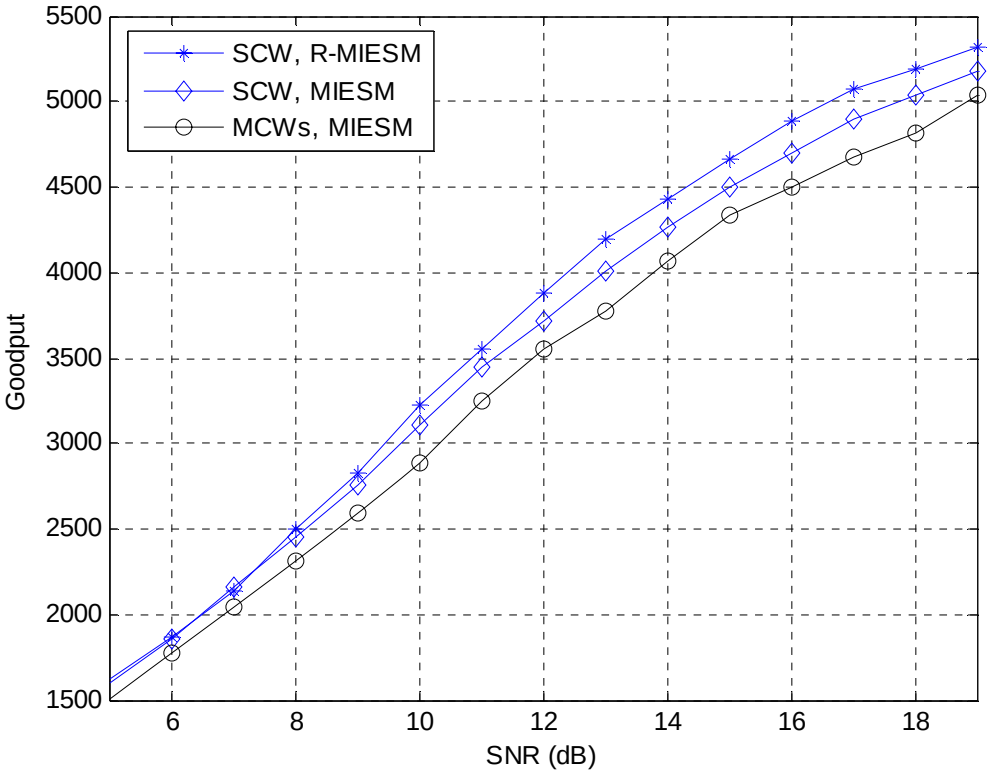

Figure 4.23: Goodput of SCW and MCWs using the MIESM scheme and the recursive MIESM scheme, with six turbo decoding iterations.

CHAPTER 5

CONCLUSIONS

This thesis proposes a novel adaptive puncturing scheme for varying the code rate within a single codeword in coded OFDMA systems. The proposed structure enables us to use longer codewords independent of the tile size. Different coding rates over the tiles are obtained through puncturing the long codeword differently on each tile. We have also proposed two channel interleaving methods for coded OFDMA systems, namely the puncturing dependant interleaver (PDI) and interleaved puncturing (IntP). In the PDI method, the size of the interleavers depends on the number of tiles that are loaded with the same rate. The IntP method uses a larger interleaver independent of the code rates used to load the different tiles. The proposed IntP structure needs further investigation regarding its joint interleaving and puncturing pattern, we leave this to be an area for future research. The proposed interleaving methods (PDI, IntP) provide larger interleaver size and thus improve the performance, specifically for constant bit rate applications. In our simulations we basically consider the PDI structure for interleaving the SCW when convolutional codes are used. For turbo codes, we only use the Turbo interleaver as in the WiMAX 802.16e standard.

We show the performance results obtained by using adaptive puncturing along with AMC. The new adaptive puncturing scheme is evaluated in case of constant and variable bit rates using Turbo and convolutional codes. For the variable bit rate, two rate selection schemes are investigated. In the first criterion, termed as recursive, the rate is selected based on the average BER calculated

according to the SNR of each subcarrier and using the non adaptive AWGN simulation to get the corresponding BER. The second scheme, termed as MIESM, the appropriate code rate and modulation order are chosen according to the effective SNR. It is observed via simulations that the SCW outperforms the MCWs and PFA using the different rate selection methods. It is also shown that MIESM provides an improved throughput for PFA, SCW and MCWs when compared to the recursive scheme. Using the MIESM rate selection scheme, the gain of the SCW over the MCWs can reach up to 25-50% at small tile sizes. The gain of SCW over the PFA is around 2-3dB; higher gains are expected over the PFA if more rates are available for the adaptive system. Analytical approximation approach for goodput estimation is introduced for the SCW and MCWs structures. The approximation has shown to be within 2dB from the simulated results.

The main advantages of the SCW over the MCWs structure are:

1. The ability to use smaller tile sizes without confining the codeword length.
2. The reduced termination overhead for convolutional codes.
3. The SCW gain over MCW is even greater using turbo codes since the turbo block size and the turbo interleaver size strongly affects performance.

A novel loading scheme for the SCW structure, termed as recursive MIESM (R-MIESM), is proposed. The scheme benefits from the high diversity the SCW provides for turbo codes. The R-MIESM scheme has shown to provide an improved goodput performance, at moderate and high SNR values, when compared to the MIESM scheme.

Further optimization of the loading scheme for the SCW is left for future investigations. The effect of the channel estimation and prediction error on the proposed adaptive structure is also left for future research.

References

1. W.Webb and R.Steele "Variable rate QAM for mobile Radio," IEEE Transactions on Communications, VOL 43, Issue 7, pp. 2223 – 2230, Jul 1995.
2. S.G.Chua and A.Goldsmith, "Variable-rate variable-power MQAM for fading channels," IEEE transaction on communications, VOL 45, pp 1218-1230, Oct 1997.
3. S.G.Chua and A.Goldsmith, "Adaptive coded modulation for fading channels," IEEE transaction on communications, VOL 46, pp 595-602, May 1998.
4. S. Vishwanath and A.Goldsmith "Adaptive Turbo-Coded Modulation for Flat Fading Channels," IEEE transaction on communications, VOL 51, NO 6, pp 964-972, Jun 2003.
5. IEEE 802.16 Broadband Wireless Access Working Group, "IEEE standard 802.16: A technical overview of the wirelessMAN air interface for broadband wireless access," 2006.
6. C.kyung, S.Chung, J.Heo, and I.Lee "Adaptive bit-interleaved coded OFDM with reduced Feedback information," IEEE transaction on communications, pp 1649-1655, Sept. 2007.
7. A. Czylwik, "Adpative OFDM for wideband radio channels," IEEE Global Telecommunication Conference (GLOBECOM'96), pp. 713-718, 1996.
8. K.Son, A.Ekbal,S.Chung, and J.Cioffi, "Adaptive modulation and coding (AMC) for bit-interleaved coded OFDM (BIC-OFDM)," IEEE transaction on wireless communications, VOL. 5, NO. 7, pp. 11685-1694, July 2006.
9. T.Keller and L.Hanzo, "Adaptive modulation technique for duplex OFDM transmission," IEEE tranaction on vehicular technology, VOL.49, NO. 5, Sept 2000.

10. X.She et al, “Power and bit allocation for adaptive Turbo coded modulation in OFDM systems,” IEEE Global Telecommunication conference (GLOBECOM’03), pp. 903-907, Dec 2003.
11. L. Ye and A.Burr, “Adaptive modulation and code rate for turbo coded OFDM transmission,” IEEE Vehicular Technology Conference, pp. 2702-2706, April 2007.
12. F.Peng, J.Zhang, and W.Ryan, “Adaptive modulation and coding for 802.11n,” IEEE Wireless Communication and Networking Conference (WCNC), pp. 656-661, Mar 2007.
13. IEEE 802.16 Broadband Wireless Access Working Group, “IEEE 802.16m Evaluation Methodology Document (EMD),” March 2008.
14. S. Simoens, S. Rouquette-Léveil, P. Sartori, Y. Blankenship and B. Classon, “Error prediction for Adaptive Modulation and Coding in Multiple-Antenna OFDM Systems,” IEEE doc., No. 802.11-03/940r4, May 2004.
15. U. Wachsmann, M. Pauli, and S. Tsai, “Quality Determination for a Communications Link,” U.S. Patent Office publication No. US 2004/0219883 A1, Nov 2004.
16. 3GPP TSG-RAM WG1 "System-level evaluation of OFDM – further considerations”, R1-031303, Nov 17-21, 2003.
17. IEEE 802.16 Broadband Wireless Access Working Group, “ CINR measurements using EESM methods,” 2005
18. K. Brueninghaus et al, “Link performance models for system level simulations of 38 broadband radio access,” IEEE PIMRC, 2005.
19. L. Wan, S. Tsai, and M. Almergn, “A fading-Insensitive Performance Metric for a Unified Link Quality Model,” IEEE wireless communication and networking conf. (WCNC), Vol.4, pp. 2110-2114, Apr 2006.
20. T.Jensen, S.Kant, J.Wehinger and B.Fleury, “Mutual information metric for fast link adaptation in IEEE 802.11n,” IEEE International Conference on Communications (ICC’08), pp.4910-4915, 2008.

21. L. Charless Lee, and C.Lee, "Convolutional coding: fundamentals and applications," 1997.
22. M.Abdelhakim, M.Nafie, A.Shalash and A.Elezabi, "Adaptive puncturing for OFDMA systems," IEEE International Conference in Communications (ICC'09), Dresden, Germany, 2009.
23. IEEE standard for local and metropolitan area network "Part 16: Air interface for fixed broadband wireless access systems," IEEE std. 802.16e, 2004.
24. R.Rollet, C.Mangin, "IEEE 802.11a, 802.11e and HiperLAN/2 Goodput Performance Comparison in Real Radio Conditions," GLOBECOM, pp. 724-728, Dec 2003.
25. S.Lin and D. Costello, "Error control coding: fundamentals and applications," second edition, 2003.
26. M.G Kim, "On systematic punctured convolutional codes," IEEE transaction on communications, VOL, 45, NO. 2, pp. 133-139, Feb 1997.
27. S. Kant and T.Jensen, "Fast link adaptation for 802.11n," Master thesis, Aalborg University, Aug 2007.
28. P.Brojesson and C.Sundberg, "Simple approximation of the error function Q(x) for communication applications," IEEE transaction in communications, VOL. COM-27, NO. 3, pp.639-643, Mar 1979.
29. IEEE 802.16 Broadband Wireless Access Working Group, "The Draft IEEE 802.16m System Description Document," Jun 2008.

APPENDIX: EXTRA SIMULATIONS

Results using convolutional codes

The different SNR thresholds used for the MCWs are listed in Table A.1. The thresholds are obtained from the AWGN simulations and by confining the codeword length to the tile size.

Table A.1: Thresholds for different tile sizes in convolutional codes for 10^{-2} BER_{target}

Tile size	Thresholds at:					
	QPSK			16QAM		
	½	2/3	¾	½	2/3	¾
3*6	0.5, 2.5, 4.5, 6.5, 9, 10					
4*6	1.5, 3, 4, 7, 9, 10.5					
5*6	1.5, 3.5, 4.5, 7, 9.5, 11					
6*6	1.5, 3.5, 4.5, 7, 9.5, 11					
9*6	2, 4, 5, 7, 9.5, 11					
18*6	2.5, 4, 5, 8, 10, 11.5					

Using the MIESM scheme and 324 carriers per frame, Figure A.1 shows the goodput performance of the SCW-PDI and MCWs at different tile sizes.

The normalized goodput per carrier for PDI-SCW and MCWs using different tile sizes and a fixed number of tiles per frame to four is shown in Figure A.2 and Figure A.3 respectively.

The estimation of goodput for the SCW and MCWs is shown in Figure A.4 and A.5 respectively, for a tile size of nine subcarries by six OFDM symbols and four tiles per frame.

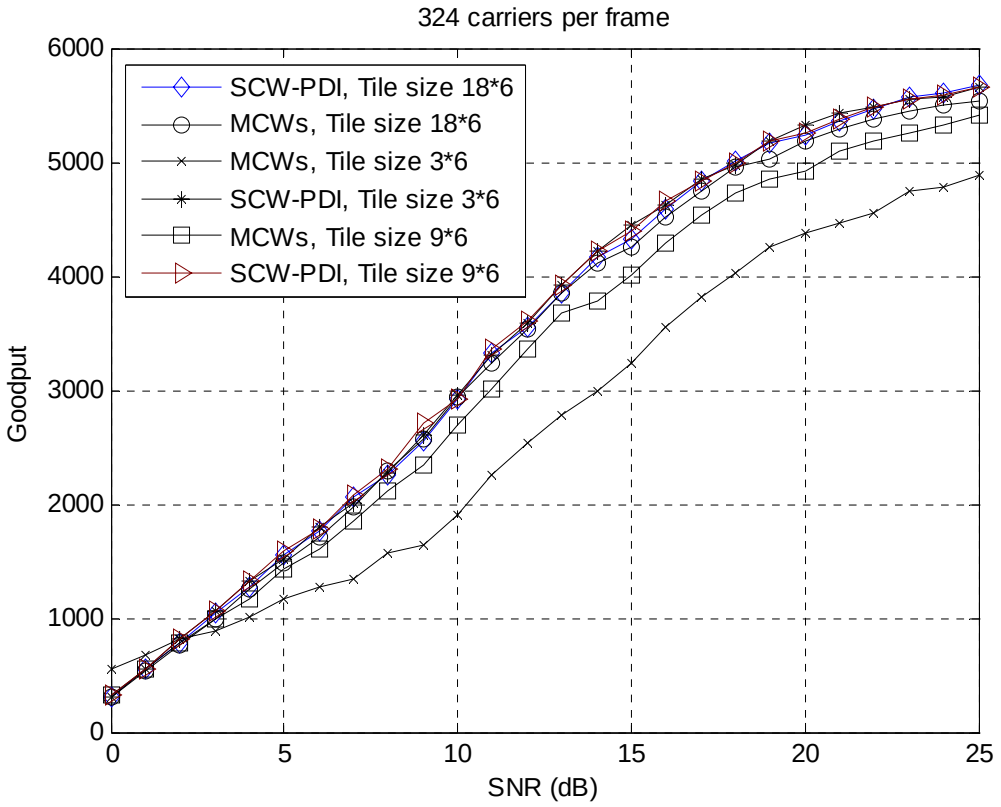

Figure A.1: Goodput performance using different tile sizes and 324 carriers per frame.

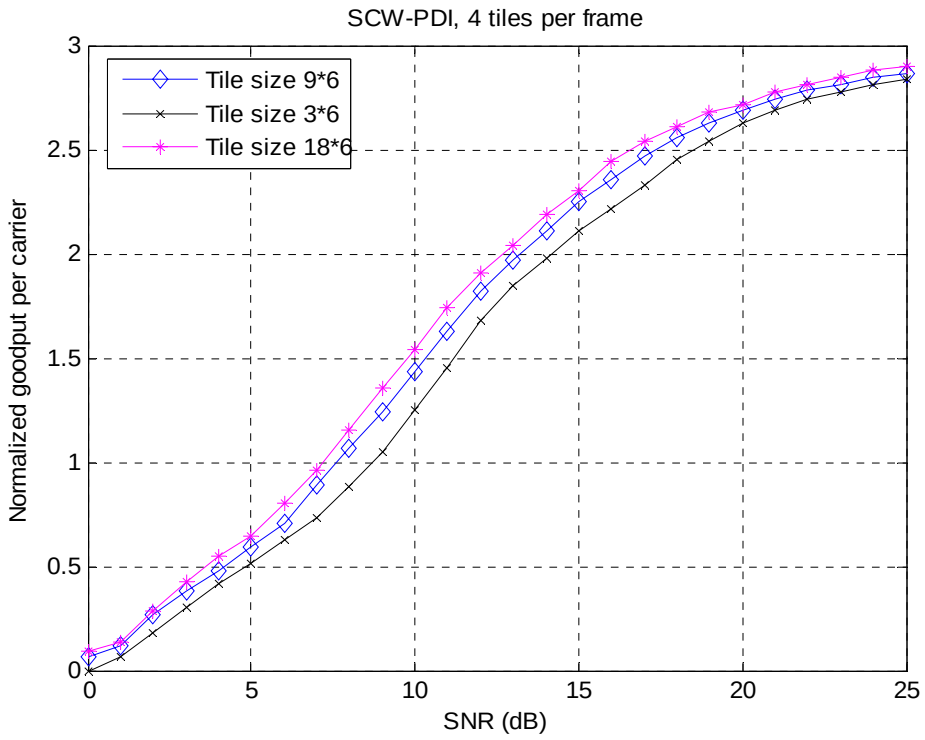

Figure A.2: Goodput for SCW using different tile sizes.

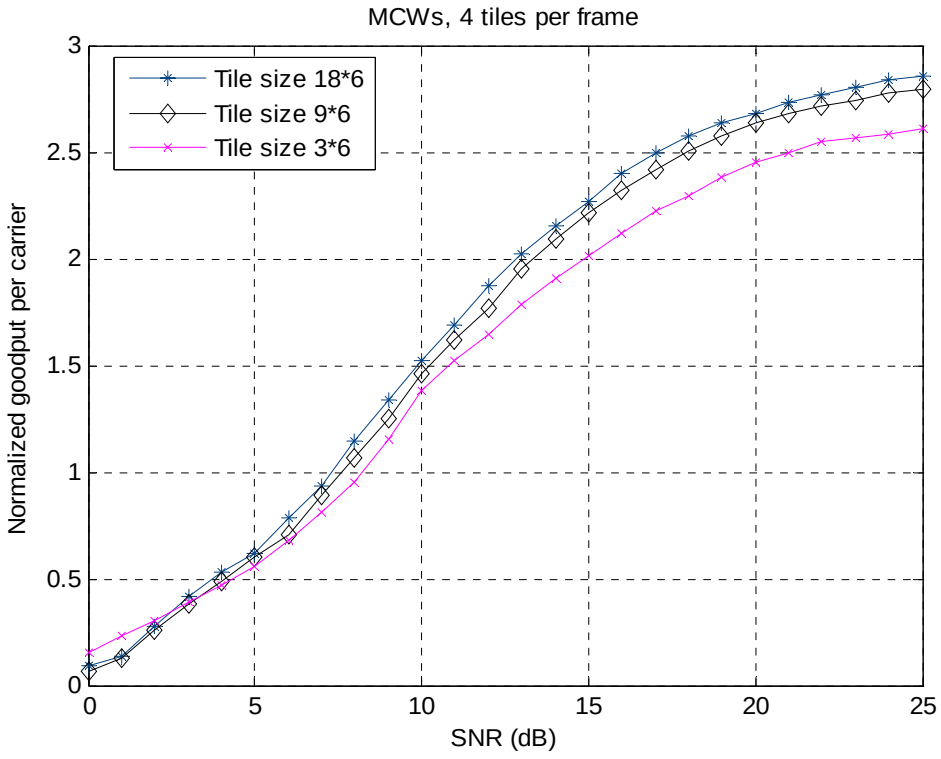

Figure A.3: Goodput for MCWs using different tile sizes.

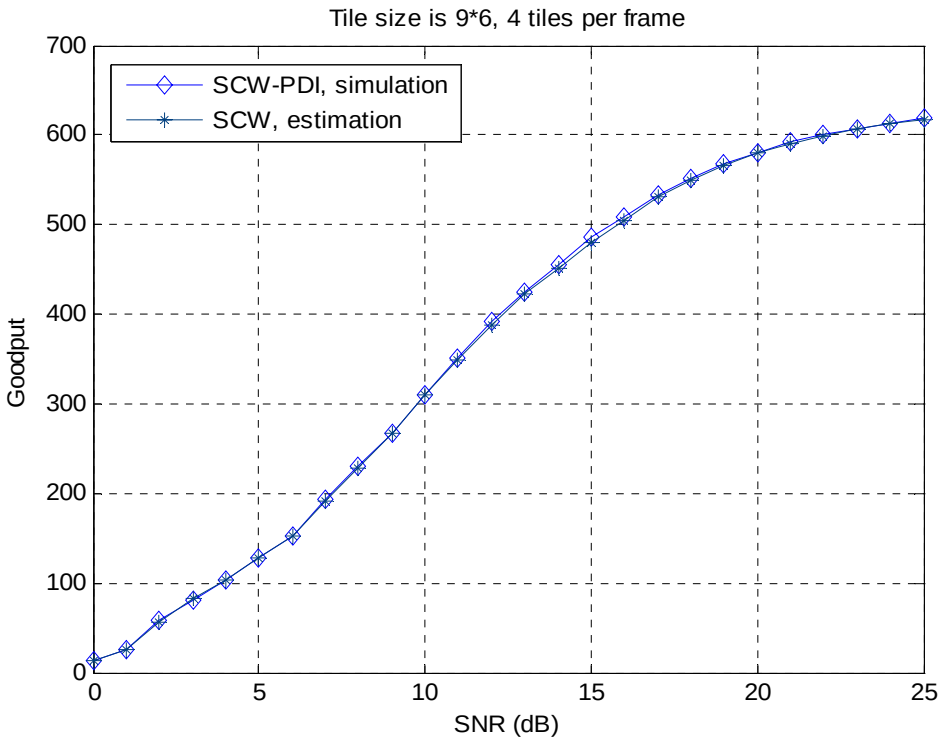

Figure A.4: Estimated and simulated goodput for SCW using 9*6 tile size.

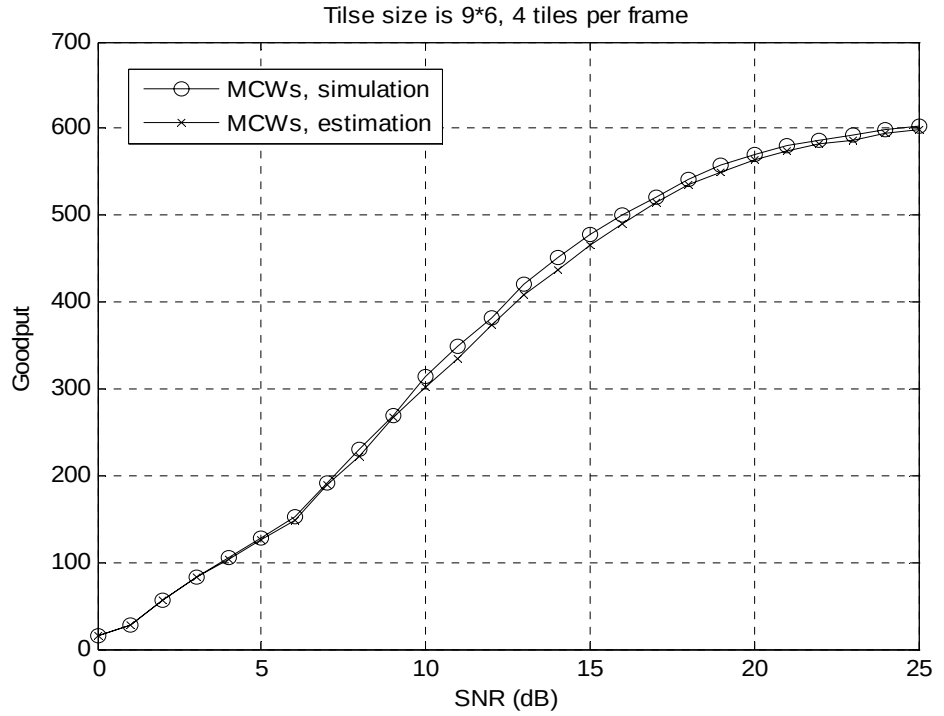

Figure A.5: Estimated and simulated goodput for SCW using 9*6 tile size.

In Figure A.6, the maximum goodput (Max GP) scheme is applied for the SCW in convolutionally coded adaptive system. The user frame is divided into 18 tiles each is 18 carriers by six symbols. In the figure we compare the maximum goodput scheme against the MIESM scheme at a target BER of 10^{-2}. It can be noticed that the MIESM scheme and Max GP scheme are achieving almost the same performance when applied to SCW. It should be noted that the PER curves used for the SCW is obtained via simulating long codewords with lengths that are equal to the frame size. However, the PER curves used for the MCWs is that obtained using short codewords that are limited to the tile size. It is shown in Figure A.7 that the MIESM scheme is achieving a better performance compared to the Max GP scheme for the MCWs.

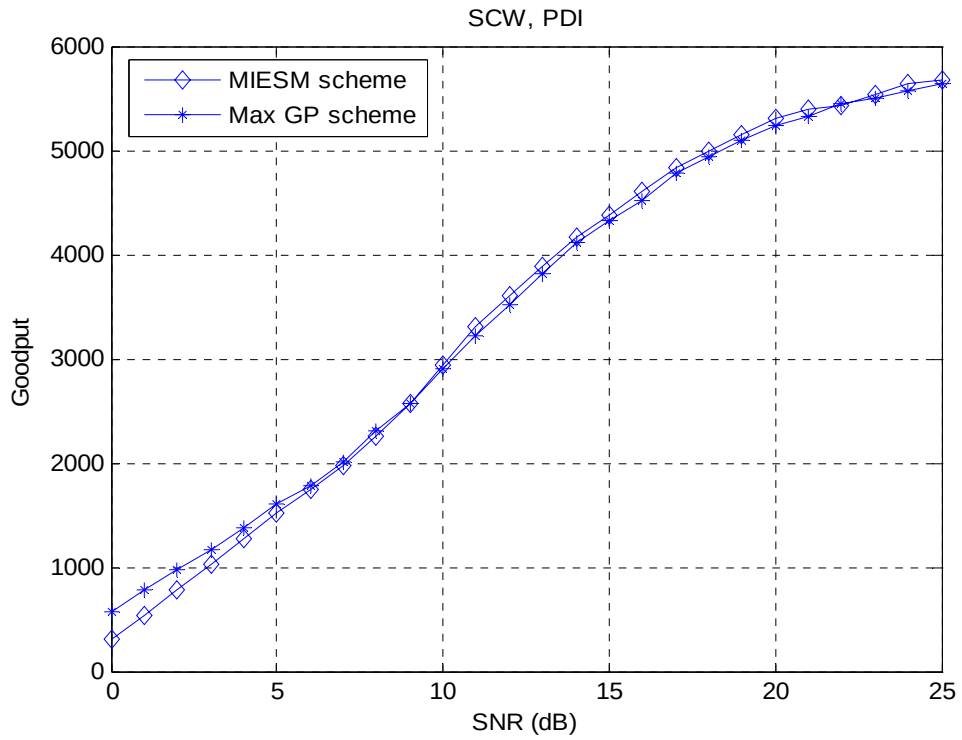

Figure A.6: Goodput of the SCW using the Max GP and MIESM schemes.

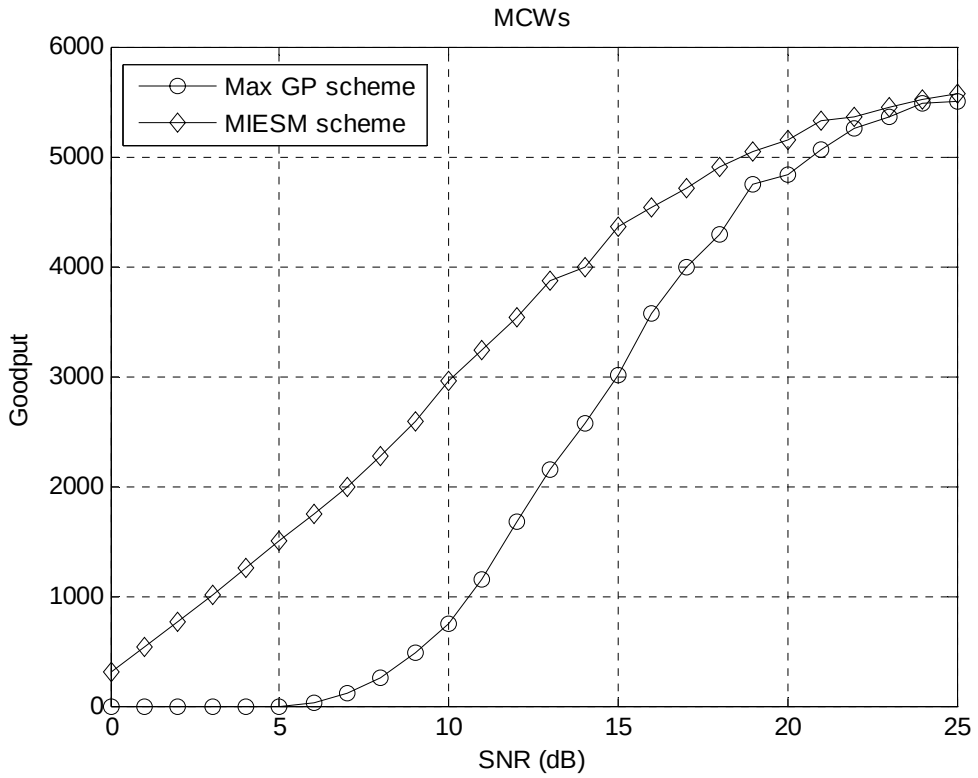

Figure A.7: Goodput of the MCWs using the Max GP and MIESM schemes.

Results using turbo codes

The AWGN switching thresholds with a turbo block size confined to the tile size is in Table A.2.

Table A.2: Thresholds for different tile sizes in Turbo codes for 10^{-2} BER_{target}

Tile size	Thresholds at:			
	QPSK		16QAM	
	½	¾	½	¾
8*6	3, 5.5, 8, 11			
16*6 and higher	2.5, 5, 7.5, 11			

Using artificial channel

Zone loading (SCW or MCW) offers more degrees of adaptation than the PFA does, thus in general it is more effective. We investigate the effectiveness of SCW against the PFA using an artificial channel. We use the MIESM scheme to determine the transmission parameters over the tiles and thus, the bit rate is variable. We set the artificial channel frequency response (*H)* as follows:

$$H = [\underbrace{1,1,\ldots 1}_{\frac{N_c}{2}}, \underbrace{\frac{1}{4},\frac{1}{4},\ldots,\frac{1}{4}}_{\frac{N_c}{2}}] \qquad \text{(A.1)}$$

where N_c is the total number of carriers.

Considering only two tiles, it is shown in Figure A.8 that a significant goodput improvement can be obtained by zone loading over the PFA. At SNR 10dB the PFA does not start any transmission while the SCW reaches a goodput of around 2900 bits.

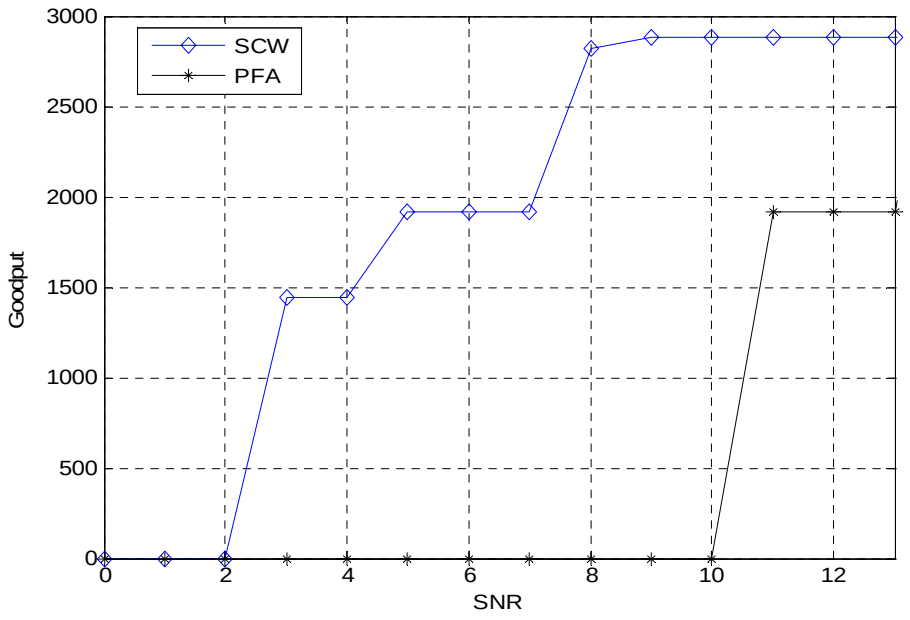

Figure A.8: Goodput performance of the SCW and PFA under the artificial channel in (A.1).

If the steps in channel variations are sharper, as in equation (A.2), the gain of zone loading becomes even higher when compared to the PFA.

$$H = [\underbrace{1,1,\ldots 1}_{\frac{N_c}{2}}, \underbrace{\frac{1}{8},\frac{1}{8},\ldots,\frac{1}{8}}_{\frac{N_c}{2}}] \qquad \text{(A.2)}$$

Using the artificial channel in (A.2) and applying the MIESM rate selection scheme, it is shown in Figure A.9 that the PFA starts transmitting at 17dB SNR value. It can be seen that the SCW has around 10dB gain over the PFA at a goodput value of 1900 bits.

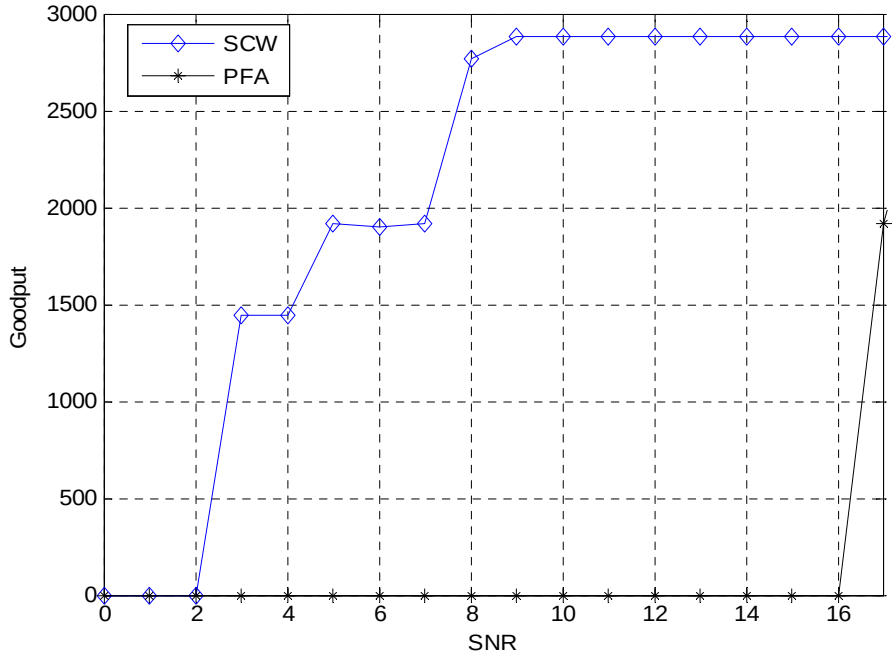

Figure A.9: Goodput performance of the SCW and PFA under the artificial channel in (A.2)

Using ITU channel

Using MIESM scheme and 160 carriers per frame, the goodput of SCW and MCWs is shown in Figure A.10 with tile sizes 8*6 and 18*6.

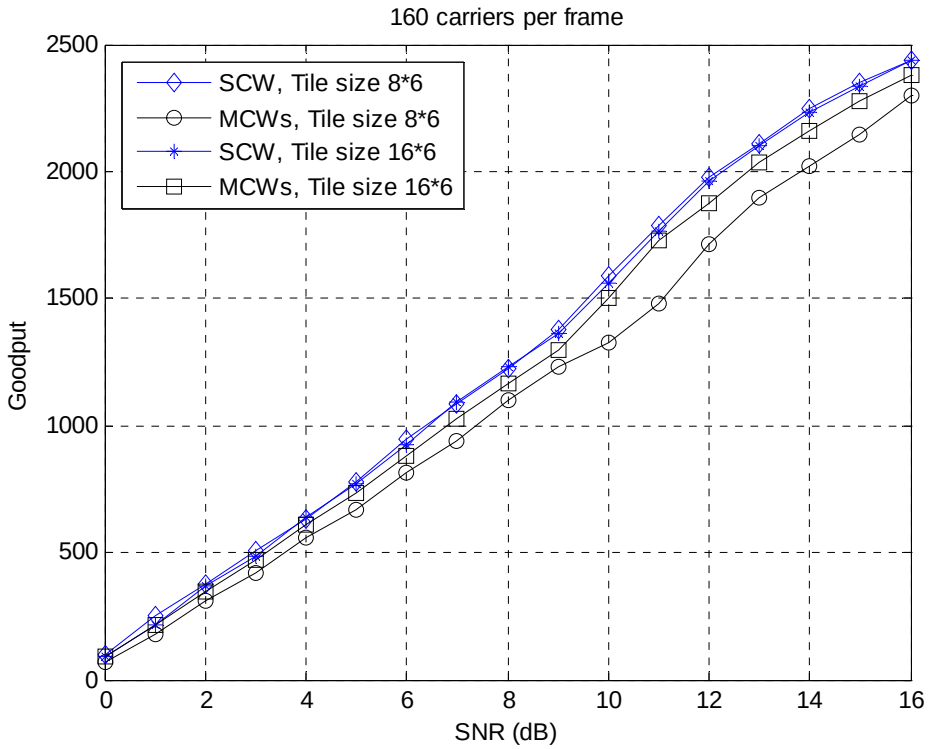

Figure A.10: Goodput of SCW and MCWs at different tile sizes.

السرعة التواؤمية في نظم الإتصالات القائمة على تقسيم الترددات المتعامدة

إعداد:

مى محمود محمد محمود عبد الحكيم

المركز القومى لبحوث وتكنولوجيا الاشعاع

هيئة الطاقة الذرية

رسالة مقدمة إلى كلية الهندسه ، جامعة القاهرة

كجزء من متطلبات الحصول على درجة الماجستير

فى هندسة الالكترونيات والاتصالات الكهربية

كلية الهندسه ، جامعة القاهرة

الجيزة ، جمهوريه مصر العربية

أبريل ٢٠٠٩

السرعة التواؤمية في نظم الإتصالات القائمة على تقسيم الترددات المتعامدة

إعداد:

مى محمود محمد محمود عبد الحكيم

المركز القومى لبحوث وتكنولوجيا الاشعاع

هيئة الطاقة الذرية

رسالة مقدمة إلى كلية الهندسه ، جامعة القاهرة

كجزء من متطلبات الحصول على درجة الماجستير

فى هندسة الالكترونيات والاتصالات الكهربية

تحت إشراف

أ.م.د. أحمد شلش

أستاذ مساعد ، بقسم هندسة الالكترونيات و الاتصالات الكهربية

كلية هندسة ، جامعة القاهرة

د. أيمن العزبى

مدرس ، بقسم هندسة الالكترونيات

كلية هندسة ، الجامعة الأمريكية بالقاهرة

كلية الهندسه ، جامعة القاهرة

الجيزة ، جمهوريه مصر العربية

أبريل ٢٠٠٩

السرعة التواؤمية في نظم الإتصالات القائمة على تقسيم الترددات المتعامدة

إعداد:

مى محمود محمد محمود عبد الحكيم

رسالة مقدمة إلى كلية الهندسه ، جامعة القاهرة

كجزء من متطلبات الحصول على درجة الماجستير

فى هندسة الالكترونيات و الاتصالات الكهربية

يُعتمد من لجنة الممتحنين:

أ.د عصام سرور	**(كلية الهندسه ، جامعة الأسكندرية)**
أ.م.د محمد نافع	**(كلية الهندسه ، جامعة القاهرة)**
أ.م.د أحمد شلش ، المشرف الرئيسى	**(كلية الهندسه ، جامعة القاهرة)**

كلية الهندسه ، جامعة القاهرة

الجيزة ، جمهوريه مصر العربية

أبريل ٢٠٠٩

ملخص الرسالة

لأن طبيعة الوسط اللاسلكى تتغير مع الزمن فإن استغلال هذة التغيرات في تواؤم سرعة النظام يحسن من أداء المنظومة المبنية. فى هذه الرسالة، يتم دراسة تغيير التحميل والتشفير أثناء الإرسال فى أنظمة تقسيم الترددات المتعامدة وذلك للتكيف مع الوضع اللحظى للوسط اللاسلكي.

فى أنظمة تقسيم الترددات المتعامدة، يمكن تطبيق نظام التواؤم على كل إطار بيانات، حيث يتم تثبيت متغيرات الإرسال الخاصة بكل إطار بينما يمكن تغييرها من إطار لآخر. إن نظام التحميل على كل مجموعة من الترددات (حزمة) في نفس إطار المعلومات يوفر مزيد من درجات التواؤم، بحيث أن كل مجموعة من حاملات التردد تُعطى نفس متغيرات الإرسال بينما المجموعات المختلفة من حاملات التردد تُعطى متغيرات مختلفة.

إن تغيير معدل التشفير لكل حزمة فى تفس الإطار يتسبب فى إرسال جمل تشفير متعددة لنفس الإطار (MCWs). في هذه الرسالة تم اقتراح طريقة لموائمة معدل التشفير فى أنظمة تقسيم الترددات المتعامدة من خلال تغيير معدل الإنقاص (Puncturing) بداخل الجملة الواحدة للتشفير(SCW) عن طريق تشفير المعلومات بأقل معدل تشفير متاح، وتقسيمها علي الحزم المختلفة ثم تتم عملية الإنقاص إعتماداً علي قياسات خاصة بجودة الوسط.

هذا ونقدم في هذه الرسالة طريقتين لتغيير ترتيب البيانات وهما PDI و IntP، والهدف منهما توفير عمق تداخل أكبر لتحسين الأداء في قنوات الخفوت.

ونقوم بدراسة طريقتين مختلفتين للتحميل والتشفير: الأولى هى طريقة تكرارية تتعامل مباشرة مع نسبة الإشارة إلى الضوضاء ، بينما الطريقة الثانية تعتمد علىالقيمة المكافئة لنسبة الإشارة إلى الضوضاء والتى يتم الحصول عليها عن طريق دالة المعلومات المشتركة. وتم اقتراح أسلوب تكراري لاختيار سرعات أعلي للطريقة الثانية.

تمت مقارنة الطريقة المقترحة (SCW) مقابل استخدام جمل شفرات متعددة (MCWs) في عملية التواؤم وأظهرت التجارب، باستخدام طرق التحميل والتشفير المختلفة، تفوق الأسلوب المقترح في الأداء.